NHS-22

NASA CR-159643

PERTURBATION SOLUTIONS OF COMBUSTION INSTABILITY PROBLEMS

by

A. Googerdy, J. Peddieson, Jr., and M. Ventrice

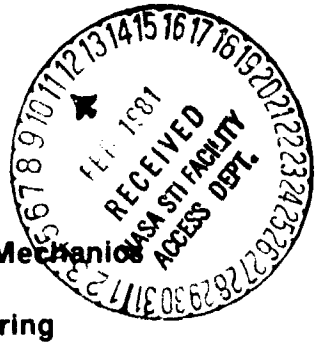

Departments of

Engineering Science and Mechanics
and
Mechanical Engineering

Tennessee Technological University
Cookeville, Tennessee 38501

Prepared for

NATIONAL AERONAUTICS AND SPACE ADMINISTRATION

NASA Lewis Research Center
Cleveland, Ohio
Contract NGR 43-003-015
R. J. Priem, Technical Monitor

FOREWORD

This report summarizes a portion of the work done on NASA Grant NGR 43-003-015. It is the masters research of the first author, Ashgar Googerdy. John Peddieson was the thesis advisor; M. Ventrice was the principal investigator of the grant.

TABLE OF CONTENTS

LIST OF FIGURES

Chapter 1

INTRODUCTION

In the operation of a liquid-propellant system the injected propellants are converted by many physical and chemical processes into hot burned gases which are accelerated to supersonic velocity by passing through a converging-diverging nozzle. Since the operation of such a system, however, is seldom perfectly smooth, the oscillations can be of either a destructive or nondestructive nature. Undestructive unsteadiness is characterized by random fluctuations in the flow properties and includes the phenomena of turbulence and combustion noise. Unsteady operation of a destructive nature, on the other hand, is characterized by organized oscillations in which there is a definite correlation between the fluctuations at two different locations in the combustor. Such oscillations have a definite frequency and result in additional thermal and mechanical loads that the system must withstand.

In liquid-propellant systems experiencing unstable combustion, heat transfer rates to the walls considerably exceed the corresponding steady state heat transfer rates, resulting in burn-out of the walls. If the system can survive these effects, mechanical vibrations in the system can cause mechanical failure or destroy the effectiveness of the delicate control and guidance systems.

The phenomenon of combustion instability depends strongly upon the unsteady behavior of the combustion process. The organized oscillations of the gas within the system must be coupled with the

combustion process in such a way as to form a feedback loop. An understanding of this coupling between the combustion process and the wave motion is necessary in order to predict the stability characteristics of the system.

There are three cases of oscillations in the combustion instability problems. The most important form of combustion instability is known as high frequency instability. As the name suggests, this type of instability represents the case of forced oscillations of the combustion chamber gases which are driven by the unsteady combustion and intract with the resonance properties of the combustion geometry. The observed frequencies, which are as high as 10,000 cycles per second, are very close to those of the natural acoustic modes of a closed-ended chamber of the same geometry as the one experiencing unstable combustion.

High frequency combustion instability can resemble any of the following acoustic modes: (1) longitudinal, (2) transverse, and (3) combined logitudinal-transverse modes. Longitudinal oscillations are usually observed in chambers whose length to diameter ratio is much greater than one; in this case the velocity fluctuations are parallel to the axis of the chamber and the disturbances depend only on one space dimension. For much shorter chambers the transverse mode of instability is most frequently observed. Transverse oscillations in rocket motors are characterized by a component of the velocity perturbation which is perpendicular to the axis of the chamber and a three-dimensional disturbance field. Such oscillations can take either of two forms: (1) the standing form in which the nodal surfaces are stationary, and (2) the spining form in which the nodal surfaces rotate in either the clockwise or counterclockwise direction.

The theoretical study of nonlinear vibration and combustion instability appears to have been initiated by a British group [1] in 1940. At that time the group testing a small solid-propellant rocket motor observed sudden increases of pressure to twice the expected level, enough to destroy a motor of flight weight. Since the early 1950's much experimental and analytical research has been developed to better understand the phenomenon of high frequency combustion instability. Most of the theories presented prior to 1966 were restricted to circumstances in which the amplitudes of the pressure oscillations were infinitesimally small, that is, in the linear regime. The case of longitudinal instability was studied by Crocco [2] as well as the studies of transverse instability by Scala [3], Reardon [4], Culick [5], and Zinn [6].

In the field of finite amplitude (nonlinear) combustion instability, mathematical difficulties have precluded any exact solutions, and approximate methods and numerical analyses have been used almost exclusively. For this reason publications in this field are relatively scarce. Notable among these is the work of Maslen and Moore [7] who studied the behavior of finite amplitude transverse waves in a circular cylinder. Their major conclusion was that, unlike logitudinal oscillations, transverse waves do not steepen to form shock waves. Maslen and Moore, however, considered only fluid mechanical effects; they did not consider the influences of the combustion process.

One of the first nonlinear analyses to include the effects of the combustion process and resulting steady state flow was performed by Priem and Guentert [8]. In this investigation the problem was made one-dimensional by considering the behavior of tangential waves

traveling in an annular section of the combustor of a liquid propellant rocket motor. In more recent years other investigators such as Burstein [9] have attempted to solve numerically the equations describing instabilities that depend on two space dimensions. Although the resulting solutions resemble experimentally observed combustion instability, this method requires excessive computer time, and studies of this type for three-dimensional oscillations will have to await the development of a much faster breed of computers. Powell [10] studied nonlinear combustion instability in liquid propellant rocket engines using the Galerkin method. He concluded that the following nonlinear mechanisms were important in determining the nonlinear stability characteristics of the system; (1) the transfer of energy between modes, (2) the self-coupling of a mode with itself, and (3) a nonlinear combustion mass source. Also Powell's work indicates that the Galerkin method can be successfully applied in the solution of nonlinear combustion instability problems. The numerical solution of the resulting ordinary differential equations will, in most cases, require much less computer time than a finite difference solution of the original partial differential equations.

The present work is motivated by a desire to determine whether or not some of the features of Powell's numerical solutions can be reproduced analytically by means of perturbation methods. For simplicity a thin rectangular chamber and a thin annular chamber are considered rather than the full cylinder investigated by Powell [10]. This eliminates one space coordinate but still allows sufficient generality to make possible the investigation of both mode-coupled annular and self-coupled rectangle instabilities. Also for simplicity

a simplified equation of state for the gas and a simplified description of the interphase mass transfer are employed. These simplifications make it unnecessary to explicitly consider the gas-phase energy equation and the fuel-drop phase balance laws. The unsteady combustion response is characterized by a simple time-delay mechanism.

The Galerkin method is used to solve the partial differential equation governing the velocity potential. This produces a set of nonlinear ordinary differential equations which are solved by singular perturbation methods. This allows limit cycles to be determined analytically and the approaches to the limit cycle to be found from simple numerical integrations.

Chapter 2

COMBUSTION EQUATIONS

It is the objective of the discussions presented in this chapter to analyze the combustor governing equations and reduce them to an analytical form that is amenable to mathematical solution. The simplification will be done in a manner that will allow the resultant equations to preserve both the mathematical and physical essence of the original problem.

The combustion chamber medium will be considered as a two-phase mixture of liquid propellant droplets and gaseous combustion products. The primary reaction between the fuel and oxidizer is assumed to occur immediately upon vaporization of the propellant droplets; that is, the vaporization process is rate controlling. Therefore, the gas phase can be treated as a single constituent. For simplicity the equation of state is assumed to have the form of a linear relation between pressure and density. The presence of burning liquid droplets in the chamber will be represented as a continuous distribution of mass sources for the gas. The burning process will be treated as history dependent, this dependence being represented by a simple time-delay mechanism.

The following equations are derived by applying the laws of conservation of mass, and momentum to an arbitrary stationary control volume. (For similar analyses see Readar [4], and Culick [5].) Because of the use of the simplified equation of state, explicit consideration

of the energy equation is not required. They are presented first in dimensional form and will be non-dimensionalized later.

Balance of mass:

$$\rho^*_{,t} + \vec{\nabla}^* \cdot (\rho^* \vec{U}^*) = \beta^* \tag{2.1}$$

Balance of momentum:

$$\rho^* (\vec{U}^*_{,t} + \vec{U}^* \cdot \vec{\nabla}^* \vec{U}^*) = -\vec{\nabla}^* P^* \tag{2.2}$$

where in equation (2.1), and (2.2) ρ^*, P^*, β^*, and $\vec{U}^*$ are the density, pressure, burning rate, and velocity in the chamber. Also $\vec{\nabla}^*$ is the dimensional gradient operator, and a comma followed by a subscripted independent variable denotes the partial derivative with respect to that variable (in this case time).

The idealized equation of state takes on the mathematical form

$$P^* = a_r^{*2} \rho^* \tag{2.3}$$

where a_r^* is the speed of sound at the reference state. Substituting (2.3) into (2.2), yields

$$\rho^* (\vec{U}^*_{,t} + \vec{U}^* \cdot \vec{\nabla}^* \vec{U}^*) = -a_r^{*2} \vec{\nabla}^* \rho^* \tag{2.4}$$

The governing equations will now be nondimensionalized with respect to a steady reference state, which will be denoted by the subscript "r." Usually this reference state is taken to be the stagnation condition at the injector face, but if the variation of

steady state properties is negligible the reference condition can be the corresponding constant steady state condition. All lengths will be referred to some characteristic length L^*. (Such as the chamber radius of a cylindrical chamber.) The characteristic velocity is the speed of sound at the reference state, and the characteristic time is the wave travel time a_r^*/L^*. The dimensionless quantities may then be written as:

$$\rho = \frac{\rho^*}{\rho_r^*} \tag{2.5}$$

$$\vec{U} = \frac{\vec{U}^*}{a_r^*} \tag{2.6}$$

$$\vec{\nabla} = L^* \vec{\nabla}^* \tag{2.7}$$

$$t = \frac{a_r^*}{L^*} t^* \tag{2.8}$$

$$p = \frac{p^*}{\rho_r^* a_r^{*2}} \tag{2.9}$$

$$\beta = \beta^* \frac{L^*}{\rho_r^* a_r^*} \tag{2.10}$$

Combining equations (2.1), (2.3), and (2.4) with equations (2.5-2.10), the dimensionless governing equations become

$$\rho_{,t} + \vec{\nabla} \cdot (\rho\vec{U}) = \beta \tag{2.11}$$

$$\vec{U}_{,t} + \vec{U} \cdot \vec{\nabla}\vec{U} = -\vec{\nabla}(\log \rho) \tag{2.12}$$

$$p = \rho \tag{2.13}$$

where "log" means natural logarithm.

It will be considerable help in the solution of the system of governing differential equations (2.11) and (2.12) if a first integral of the momentum equation can be found. This can be accomplished if the flow is irrotational, because the velocity vector can then be expressed as the gradient of a scalar potential. Under these conditions it is possible to combine the equations to obtain a single partial differential equation governing the behavior of the velocity potential. The pressure is then related to the velocity potential by the integrated momentum equation. To prove that flow is irrotational, it can be done by taking "curl" from equation (2.12) and also using the vector identities

$$\vec{\nabla} \cdot (\vec{\nabla} \times F) = 0$$

$$\vec{\nabla} \times (\vec{\nabla} A) = 0$$

$$\vec{F} \times (\vec{\nabla} \times \vec{F}) = \vec{\nabla}(\tfrac{1}{2} F^2) - \vec{F} \cdot \vec{\nabla}\vec{F}$$

to find

$$\frac{D\vec{W}}{Dt} = \vec{W} \cdot \vec{\nabla}\vec{U} - (\vec{\nabla} \cdot \vec{U})\, \vec{W} \tag{2.14}$$

where $\vec{W}$ is vorticity vector, and defined by

$$\vec{W} = \vec{\nabla}\times\vec{U} \tag{2.15}$$

Equation (2.14) can be satisfied by

$$\vec{W} = 0 \tag{2.16}$$

which will be true provided

$$\vec{W}(\vec{r},0) = 0 \tag{2.17}$$

therefore equation (2.16) shows that flow is irrotational.

Introducing the velocity potential defined by

$$\vec{U} = \vec{\nabla}\psi \tag{2.18}$$

substituting (2.18) into (2.12) and (2.11) yields

$$\rho = \bar{e}^{(\psi_{,t} + \frac{1}{2}\vec{\nabla}\psi \cdot \vec{\nabla}\psi)} \tag{2.19}$$

$$\rho_{,t} + \rho\nabla^2\psi + \vec{\nabla}\psi \cdot \vec{\nabla}\rho = \beta \tag{2.20}$$

Due to their nonlinear natures the system of wave equations (2.19) and (2.20) cannot be solved exactly. In order to obtain simpler, but approximate, form, an order of magnitude analysis will be performed to determine which terms can be neglected. In this approximation scheme each perturbation quantity will be assigned the order of magnitude $0(\varepsilon)$ where ε is a measure of the magnitude of the initial disturbance. It then follows that products of perturbation quantities are of second order or $0(\varepsilon^2)$. To obtain an equation that is correct to a given order

all terms of higher order are neglected. By this definition it is seen that first order equations are necessarily linear.

The equations derived from this perturbation analysis are expected to be valid as long as the amplitude of the perturbation quantities is finite but smaller than unity. If in addition it is assumed that the Mach number of the steady state flow is small, additional terms can be neglected. The behavior of the steady state quantities is governed by the time independent versions of equations (2.19) and (2.20). Setting the time derivatives equal to zero, and retaining only terms of 0 (1) and 0(ε) yields the steady-state equations. Substituting into these

$$\psi = \varepsilon\bar{\phi}(z) \tag{2.21}$$

$$\beta = \bar{\beta}(z) \tag{2.22}$$

$$\bar{\beta} = 0(\varepsilon) \tag{2.23}$$

and letting

$$\beta = \bar{w} = \varepsilon\bar{\sigma} \tag{2.24}$$

yield

$$\rho = 1 - \frac{1}{2}\varepsilon^2\left(\frac{d\bar{\phi}}{dt}\right)^2 + \cdots \tag{2.25}$$

$$\frac{d^2\bar{\phi}}{dz^2} - \frac{3}{2}\varepsilon^2\left(\frac{d\bar{\phi}}{dz}\right)^2\frac{d^2\bar{\phi}}{dz^2} + \cdots = \bar{\sigma} \tag{2.26}$$

For $\varepsilon \ll 1$ (2.26) reduce to

$$\frac{d^2\bar{\phi}}{dz^2} = \bar{\sigma} \tag{2.27}$$

It will be assumed that the combustion is uniformly distributed. $\bar{w}$ is constant, therefore (2.27) can be integrated to find steady state velocity distribution

$$\bar{U} = \bar{\sigma}z + c \tag{2.28}$$

$$\bar{U}(0) = 0 \tag{2.29}$$

thus

$$\bar{U} = \bar{\sigma}z \tag{2.30}$$

The complete velocity potential is now defined by sum of steady state and unsteady state contribution, and a second order analysis will be performed on the simplified wave equation [i.e. eqs. (2.19-2.20)] to obtain a set of second order equation involving the velocity potential. After a first integral of the momentum equation is obtained these equations will be combined to yield a single nonlinear differential equation governing the behavior of the velocity potential. To this end let

$$\psi = \varepsilon(\bar{\phi} + \phi(x,y,z,t)) \tag{2.31}$$

$$\beta = \bar{w} + \varepsilon w = \varepsilon(\bar{\sigma} + \varepsilon\sigma) \tag{2.32}$$

substituting (2.31) into (2.19) yields

$$\rho = 1 - \varepsilon\phi_{,t} + \frac{1}{2}\varepsilon^2[(\phi_{,t})^2 - (\bar{\sigma}^2 + \vec{\nabla}\phi \cdot \vec{\nabla}\phi) - 2\bar{\sigma}\phi_{,z}] + \text{----} \qquad (2.33)$$

substituting (2.33) and (2.31) into (2.20) yields

$$\phi_{,tt} - \nabla^2\phi + \varepsilon[\bar{\sigma}\phi_{,t} + 2\bar{\sigma}\phi_{,tz} + 2\vec{\nabla}\phi \cdot \vec{\nabla}(\phi_{,t}) + \sigma] = 0 \qquad (2.34)$$

note that

$$\phi_{,tt} = \nabla^2\phi + 0(\varepsilon) \qquad (2.35)$$

It is to be noted that equation (2.34) has the form of an inhomogeneous wave equation.

Substituting (2.35) into (2.34) yields

$$\phi_{,tt} - \nabla^2\phi + \varepsilon(\bar{\sigma}\phi_{,t} + 2\vec{\nabla}\phi \cdot \vec{\nabla}(\phi_{,t}) + \sigma) = 0 \qquad (2.36)$$

To roughly account for changes in the frequency spectrum due to baffles, cavities, etc., the governing equation will be modified as follows

$$\phi_{,tt} - \nabla^2\phi + \varepsilon(\bar{\sigma}\phi_{,t} + 2\vec{\nabla}\phi \cdot \vec{\nabla}(\phi_{,t}) - \kappa\nabla^2(\phi_{,tt}) + \sigma) = 0 \qquad (2.37)$$

where the term multiplied by κ is a correction factor. This can also be written as

$$\phi_{,tt} + \bar{w}\phi_{,t} - \nabla^2\phi + 2\varepsilon(\vec{\nabla}\phi \cdot \vec{\nabla}(\phi_{,t}) - \kappa\nabla^2(\phi_{,tt})) = -w \qquad (2.38)$$

Chapter 3

COMBUSTION IN A THIN RECTANGULAR CHAMBER

In this chapter the modified form of the governing equation (2.36) will be used to study the effect of nonlinearities on the stability of a thin rectangular chamber in which the distributed combustion process is that described by Croco [2]. For simplicity one dimensional instabilities will be considered for a combustor geometry with uniformly distributed injection (see Fig. 1). In this case all lengths are referred to characteristic length L^*, the chamber length.

The dimensionless coordinates may then be written as:

$$x = \frac{x^*}{L^*} \tag{3.1}$$

$$y = \frac{y^*}{L^*} \tag{3.2}$$

$$z = \frac{z^*}{L^*} \tag{3.3}$$

Therefore, the nondimesional combustor geometry is given by Fig. 2.

To formulate the combustion function it is first necessary to recall that the dimensionless pressure perturbation can be expressed as:

$$q = \frac{p - p_0}{p_0 \varepsilon} = -\phi_{,t} + O(\varepsilon) \tag{3.4}$$

The combustion process is assumed to be described by the pressure-sensitive time-delay model developed by Crocco [2] and employed by Powell [10].

In the present notation this can be written as:

$$\sigma = \bar{\sigma} n(q - q_T), q_T = q(t - T) \tag{3.5}$$

where n is called the interaction index (a measure of the strength of the combustion process) and T is called the (dimensionless) time-delay parameter (a measure of the importance of history effects).

The governing equation (2.36) now becomes:

$$\phi_{,tt} - \nabla^2\phi + \varepsilon(\bar{\sigma}((1 - n)\phi_{,t} + n(\phi_T)_{,t}) + 2\vec{\nabla}\phi \cdot \vec{\nabla}(\phi_{,t})$$

$$-\kappa\nabla^2(\phi_{,tt})) + O(\varepsilon^2) = 0 \tag{3.6}$$

It is now necessary to select a potential function to predict the behavior of the amplitutes of the various acoustic modes of the chamber. As a first approximation attention will be restricted to the first term of a Fourier series, satisfying the boundary condition at $y = \pm\pi/2$, that is

$$\phi(y,t) = F(t)\sin y \tag{3.7}$$

Substituting (3.7) into (3.6) (and letting $\kappa = 0$ for simplicity) yields

$$\dot{F}^{\cdot} + F + \epsilon(\bar{\sigma}(1 - n)\dot{F} + n\dot{F}_T) + 8/3\pi F\dot{F}) + 0(\epsilon^2) = 0 \qquad (3.8)$$

where

$$(\dot{}) = d(\ )/dt$$

Equation (3.8) has the same mathematical form as the equation obtained by Powell [10] in his study of purely radial instability in a cylindrical combustion chamber. His numerical solutions showed that the stability of the solution depended on the initial amplitude of the disturbance. Powell [10] also found some cases which were classified as stable by the linear theory were predicted to be unstable by the nonlinear theory and vice-versa. In the present work a combination of the two-variable and strained-parameters perturbation methods (see, for instance Nayfeh [11]) will be used to obtain approximate closed-form solution to (3.8) which will be used to explain the behavior discovered by Powell [10].

Let,

$$\epsilon_1 = 8\epsilon/3\pi \qquad (3.9)$$

To begin the two-variable perturbation process, let

$$\xi = t \qquad (3.10)$$

$$\eta = \epsilon t \qquad (3.11)$$

and subtitute (3.9), (3.10), and (3.11) into (3.8) to get:

$$F_{,\xi\xi} + F + \epsilon_1 FF_{,\xi} + \epsilon(2F_{,\xi\eta} + \bar{\sigma}((1 - n)F_{,\xi} + n(F_T)_{,\xi})) + 0(\epsilon^2) = 0 \qquad (3.12)$$

Assuming

$$F = F_0 + \varepsilon F_1 + 0(\varepsilon^2) \tag{3.13}$$

the governing equation for first and second order approximations can be readily written as:

$$F_{0,\xi\xi} + F_0 + \varepsilon_1 F_0 F_{0,\xi} = 0 \tag{3.14}$$

$$F_{1,\xi\xi} + F_1 + \varepsilon_1 (F_0 F_{1,\xi} + F_1 F_{0,\xi})$$

$$= -(2F_{0,\xi\eta} + \bar{\sigma}((1 - n)F_{0,\xi} + n(F_{0T}),_{\xi}))$$

$$+ 0(\varepsilon^2) = 0 \tag{3.15}$$

An approximate solution to (3.14) will now be found by using the method of strained-parameters with ε_1 as the perturbation parameter. Toward this end let

$$\xi = (1 + \varepsilon_1^2 W_1 + \text{----})z \tag{3.16}$$

substituting (3.16) into (3.14), and assuming

$$F_0 = F_{00} + \varepsilon_1 F_{01} + \varepsilon_1{}^2 F_{02} + 0(\varepsilon^3) \tag{3.17}$$

yields

$$F_{00,zz} + F_{00} = 0 \tag{3.18}$$

$$F_{01,zz} + F_{01} = -F_{00} F_{00,z} \tag{3.19}$$

$$F_{02,zz} + F_{02} = -F_{00}F_{01,z} - F_{01}F_{00,z} + 2W_1F_{00,zz} \tag{3.20}$$

It is assumed that the solution equation (3.18) can be written as:

$$F_{00} = C(\eta)\cos(z - \alpha(\eta)) \tag{3.21}$$

where $C(\eta)$, and $\alpha(\eta)$ are the amplitude and phase angle respectively.

Substituting (3.21) into (3.19), and finding a particular solution of the resulting equation yields

$$F_{01} = -1/6\ C^2\sin 2(z - \alpha) \tag{3.22}$$

and substituting (3.21) and (3.22) into (3.20) yields

$$F_{02,\xi\xi} + F_{02} = (1/12\ C^2 - 2W_1)C\cos(z - \alpha) + 1/4\ C^3\cos 3(z - \alpha) \tag{3.23}$$

The particular solution corresponding to the first term on the right hand side will be proportional to $z\sin(z - \alpha)$. Thus limit

$$\frac{F_{02}}{F_{00}} = \infty$$

as z goes to ∞ (violating the basic assumption of the perturbation process, namely that $\epsilon_1 F_{01}$ and $\epsilon_1^2 F_{02}$ represent small correction to F_{00}) unless this term vanishes. Thus

$$W_1 = 1/24\ C^2 \tag{3.24}$$

Substituting (3.24) and (3.16) into (3.21) yields

$$F_{00} = C\cos((1 - 1/24\ \epsilon_1^2 C^2)\xi - \alpha) + 0(\epsilon_1) \tag{3.25}$$

Note,

$$F_0 = F_{00} + 0(\epsilon_1) \tag{3.26}$$

Now by substituting (3.26) into (3.15) and using the fact that:

$$\sin(A - B - C) = \sin(A - B)\cos C - \cos(A - B)\sin C$$

one finds that

$$F_{1,\xi\xi} + F_1 = (2\frac{dC}{d\eta} + \bar{\sigma}((1 - n)C + nC\cos(1 - \frac{1}{24}\epsilon_1^2 C^2)T))\cdot$$

$$\sin((1 - \frac{1}{24}\epsilon_1^2 C^2)\xi - \alpha) - C(2\frac{d\alpha}{d\eta} + \bar{\sigma}n\sin(1 - \frac{1}{24}\epsilon_1^2 C^2)T)\cdot$$

$$\cos((1 - \frac{1}{24}\epsilon_1^2 C^2)\xi - \alpha) \tag{3.27}$$

Eliminating singularity and using (3.9) and (3.11) yields

$$\dot{C} + \frac{1}{2}\epsilon\bar{\sigma}C(1 - n(1 - \cos(1 - \frac{8}{27\pi^2}\epsilon^2 C^2)T)) = 0 \tag{3.28}$$

$$\dot{\alpha} + \frac{1}{2}\epsilon\bar{\sigma}n\sin(1 - \frac{8}{27\pi^2}\epsilon^2 C^2)T = 0 \tag{3.29}$$

The linear stability analysis can be recovered from (3.28) and (3.29) by neglecting the nonlinear terms in the arguments of the trigonometric functions. This yields

$$\dot{C} + \frac{1}{2}\epsilon\bar{\sigma}C(1 - n(1 - \cos T)) = 0 \tag{3.30}$$

$$\dot{\alpha} + \frac{1}{2}\epsilon\bar{\sigma}n\sin T = 0 \tag{3.31}$$

with initial conditions

$$C(0) = 1 \tag{3.32}$$

$$\alpha(0) = 0 \tag{3.33}$$

The appropriate closed-form solutions can be written as:

$$C = e^{-\epsilon\bar{\sigma}(1 - n(1 - \cos T))t/2} \tag{3.34}$$

$$\alpha = -\frac{1}{2}(\epsilon\bar{\sigma}n\sin T)t \tag{3.35}$$

It can be seen that perturbation in C will decay for

$$n < \frac{1}{1-\cos T} \tag{3.36}$$

thus

$$n = \frac{1}{1 - \cos T} \tag{3.37}$$

is the neutral stability curve according to the linear theory (Fig. 3).

Equations (3.28) and (3.29) must be solved numerically. To get an idea of the behavior that will be predicted by numerical analysis, it is instructive to obtain approximate closed-form solutions to (3.28) and (3.29). This can be done by expanding the trigonometrical functions appearing therein and retaining only the first terms to get

$$\dot{C} + \frac{1}{2}\epsilon\bar{\sigma}C(1 - n(1 - (\cos T + \frac{8}{27\pi^2}\epsilon^2 T\sin TC^2))) = 0 \qquad (3.38)$$

$$\dot{\alpha} + \frac{1}{2}\epsilon\bar{\sigma}n(\sin T - \frac{8}{27\pi^2}\epsilon^2 T\cos TC^2) = 0 \qquad (3.39)$$

The initial conditions remain

$$C(0) = 1 \qquad (3.40)$$

$$\alpha(0) = 0 \qquad (3.41)$$

Eauations (3.38) and (3.39) may be written as the form

$$\dot{C} - aC + bC^3 = 0 \qquad (3.42)$$

$$\dot{\alpha} + eC^2 + i = 0 \qquad (3.43)$$

where a, b, e, and i are

$$a = -\frac{1}{2}\epsilon\bar{\sigma}(1 - n(1 - \cos T)) \qquad (3.44)$$

$$b = \frac{4}{27\pi^2}\epsilon^3\bar{\sigma}nT\sin T \qquad (3.45)$$

$$e = -b\cot T \qquad (3.46)$$

$$i = \frac{1}{2}\epsilon\bar{\sigma}n\sin T \qquad (3.47)$$

The solutions of Equations (3.42) and (3.43) can be written as:

$$C(t) = \overset{+}{e}^{at}\sqrt{\frac{a}{a - b(1 - \overset{+}{e}^{2at})}} \tag{3.48}$$

$$\alpha(t) = -\frac{\cot T}{2}\ln[1 - \frac{b}{a}(1 - \overset{+}{e}^{2at})] - it \tag{3.49}$$

Information about the behavior of the solutions obtained in this chapter is conveniently illustrated by considering stability boundaries plotted in the n - T plane. By setting

$$\dot{C} = 0 \tag{3.50}$$

in (3.28), the equation

$$n_E = \frac{1}{1 - \cos(1 - \frac{8\epsilon^2}{27\pi^2}C^2)T} \tag{3.51}$$

is obtained. This is the nonlinear neutral-stability curve. For pairs of values of n and T satisfying this equation the amplitude of the solution will remain fixed for all values of time. If ϵ is equated to zero in (3.51) the linear neutral-stability equation

$$n_L = \frac{1}{1 - \cos T} \tag{3.52}$$

is obtained. If (3 51) is expanded for $\frac{8\epsilon^2}{27\pi^2} \ll 1$ one obtains the approximate neutral-stability curve

$$n_A = \frac{1}{1 - \cos T - \frac{8\epsilon^2}{27\pi^2} T\sin T} \tag{3.53}$$

This corresponds to the approximate solution (3.48). Figures 4 and 5 show plots of (3.51) and (3.53) respectively for the same values of ε. It can be seen that for $\varepsilon \leq 1$ the two sets of curves are in close agreement. In fact, numerical computations have shown that for $\varepsilon \leq \frac{1}{2}$ equations (3.51) and (3.53) produce results that are practically indistinguishable in the region $0 \leq T \leq 2\pi$. This suggests that the approximate solution (3.48) is likely to be a good approximation to the exact numerical results for moderate values of ε. In what follows the validity of this hypothesis will be demonstrated.

To an exaggerated scale typical curves plotted in Figure 4 looks as follows.

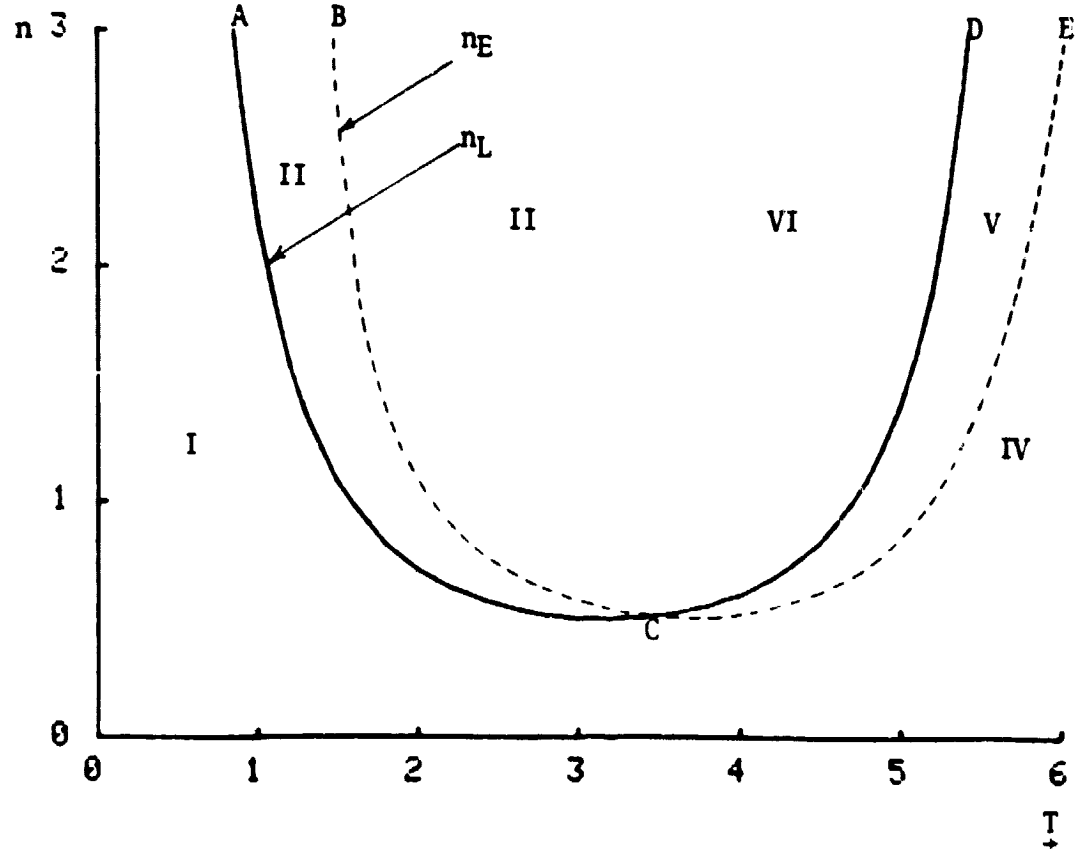

The stability diagram can be conveniently divided into six regions as shown above. There are

I: $T<\pi$, $n<n_L$

II: $T<\pi$, $n_L<n<n_E$

III: $T<\pi$, $n>n_E$

IV: $T>\pi$, $n<n_E$

V: $T>\pi$, $n_E<n<n_L$

VI: $T>\pi$, $n>n_L$

The approximate solution (3.48) will now be used to infer the behavior of the solution in each region. Then some exact numerical results will be examined. The approximate equations are repeated below:

$$c = \frac{e^{at}}{\sqrt{1 - \frac{b}{a}(1 - e^{2at})}} \tag{3.54}$$

$$a = \frac{1}{2}\epsilon\bar{\sigma}(n(1 - \cos T) - 1) = \frac{1}{2}\epsilon\bar{\sigma}(\frac{n}{n_L} - 1) \tag{3.55}$$

$$b = \frac{4\epsilon^3}{27\pi^2}nT\sin T \tag{3.56}$$

The stability boundary corresponds to a = b.

In region I a<0, b>0. Substituting $a = -a_1$ into (3.54) yields

$$C = \frac{e^{-a_1 t}}{\sqrt{1 + \frac{b}{a_1}(1 - e^{-2a_1 t})}} \tag{3.57}$$

It can be seen that

$$\lim_{t \to \infty} C = 0 \tag{3.58}$$

Thus the amplitude decays to zero in region I. In region II $a>0$, $b>0$ and $a<b$. In region III $a>0$, $b>0$ and $a>b$. In either case (3.54) implies

$$\lim_{t \to \infty} C = \sqrt{\frac{a}{b}} \tag{3.59}$$

It can be seen that in both region II and region III a limit-cycle is approached. For region II the amplitude of the limit-cycle is less than that of the initial amplitude while for region III the limit-cycle amplitude is greater than the initial amplitude. For $a = b$ (3.54) reduces to

$$C = 1 \tag{3.60}$$

which is the solution associated with the nonlinear stability curve.

In region IV $a<0$, $b<0$ and $a<b$. In region V $a<0$, $b<0$ and $a>b$. Substituting $a = -a_1$ and $b = -b_1$ into (3.54) one obtains

$$C = \frac{e^{-a_1 t}}{\sqrt{1 - \frac{b_1}{a_1}(1 - e^{-2a_1 t})}} \tag{3.61}$$

where for region IV $a_1>b_1$ and for region V $a_1<b_1$. For the former region it is possible to take the limit as t goes to infinity to get

$$\lim_{t \to \infty} C = 0 \tag{3.62}$$

In region IV, therefore, the amplitude decays to zero. For the latter region, on the other hand, the corresponding limit can not be taken because C becomes infinite in a finite time. Denoting this time by t_∞ it can be seen from (3.61) that

$$1 - \frac{b_1}{a_1}(1 - e^{-2a_1 t_\infty}) = 0 \quad \text{or}$$

$$t_\infty = -\frac{1}{2a_1}\ln(1 - \frac{a_1}{b_1}) \tag{3.63}$$

If $a_1 = b_1$ (3.63) reduces to

$$C = 1 \tag{3.64}$$

which corresponds to neutral stability.

In region VI $a>0$ and $b<0$. Substituting $b = -b_1$ into (3.54) yields

$$C = \frac{e^{at}}{\sqrt{1 - \frac{b_1}{a}(e^{2at} - 1)}} \tag{3.65}$$

In this case C becomes infinite when $t = t_\infty$ where

$$1 - \frac{b_1}{a}(e^{2at_\infty} - 1) = 0 \quad \text{or}$$

$$t_\infty = \frac{1}{2a}\ln(1 + \frac{a}{b_1}) \tag{3.66}$$

Near the linear stability curve $|a|<<1$. Expanding (3.63) and (3.66) in this region one finds that

$$(t_\infty)_V = +\frac{1}{2b_1}\left(1 + \frac{a_1}{2b_1} + \text{----}\right) \tag{3.67}$$

$$(t_\infty)_{VI} = \frac{1}{2b_1}\left(1 - \frac{a}{2b_1} + \text{----}\right) \tag{3.68}$$

Thus,

$$(t_\infty)_{VI} < (t_\infty)_V .$$

The results obtained in regions V and VI violate the condition of validity of (3.54), namely that the magnitude of C be moderate. Thus the information obtained about the behavior of the solution in this region can be used only in a qualitative sense. Nevertheless, as will be seen, (3.61) and (3.65) correctly predict the main feature of exact solution.

To summarize, the following behavior has been found based on the approximate solution (3.53). Below curve ACE (regions I and IV) all disturbances decay to zero. Above curve ACE the behavior of the solution depends on the value of T. For $T<\pi$ all disturbances evolve into limit cycles. In region II the value of the final amplitude is less than that of the initial amplitude, while in region III the situation is reversed. For $T>\pi$ all disturbances increase without bound. The rate of increase is slower for region V than for region VI.

Some typical numerical results obtained by solving equation (3.28) by a fourth-order Runge-kutta method are shown in Figures 6-9. Figure 6 shows three sets of data obtained along the line n = 1 in the vicinity of $T = \frac{\pi}{2}$ (the curves are labeled in degrees rather than radians to better bring out the small differences in the values of T that were used). Each curve is representative of a different parametric region which is included in the labeling of each curve. It can be seen that these results are in qualitative agreement with the predictions of the approximate solution. Other results, not shown, reveal that the amplitude of the limit-cycle in region III increases rapidly as T increases. Such large limit-cycles are probably inconsistent with the order of magnitude assumption inherent in the perturbation method and, therefore, will not be discussed.

Figure 7 shows three sets of data obtained along the line $T = \frac{\pi}{2}$ in the vicinity of n = 1. The results for regions I and III are again in complete qualitative agreement with the approximate solution. It can be seen that the longest decay time is exhibited by data corresponding to a point on the borderline between regions I and II. The corresponding result based on the approximate analysis is found by taking the limit of (3.54) as $a \to 0$ to get

$$C = \frac{1}{\sqrt{1 + 2bt}} \tag{3.69}$$

Since the decay in this case is algebraic rather than exponential (as it is for $a \neq 0$) this case will exhibit the slowest decay in agreement with the exact solution.

Figure 8 shows three sets of data obtained along the line $n = 1$ in the vicinity of $T = \frac{3\pi}{2}$. The case corresponding to region IV decays to zero in agreement with the approximate solution. In regions V and VI, however, the disturbances evolve into limit cycles rather than growing without bound as predicted by the approximate analysis. In contrast to the situation for $T<\pi$, it does not appear possible to find any values of T for which the limit-cycle amplitude will have a moderate value. Since the accuracy of solutions exhibiting large limit-cycle amplitude is doubtful, the difference between the unbounded growth predicted by the approximate solution and the growth to a very large limit cycle predicted by the exact analysis is probably unimportant. It can be seen that the rate of growth of the solution increases as one proceeds from region IV to region VI as predicted by the approximate solution.

Figure 9 shows two sets of data obtained along the line $T = \frac{3\pi}{2}$ in the vicinity of $n = 1$. Again the differences in behavior between regions IV and VI are clearly illustrated.

Powell [10] observed similar behavior to that discussed above in his numerical solutions to an equation similar to (3.28). The perturbation analysis given here makes it clear that the main effect causing the observed behavior is the frequency shift due to nonlinear amplitude-frequency dependence and the accompanying distortion of the neutral stability curves in the n - T plane.

Chapter 4

COMBUSTION IN A THIN ANNULAR CHAMBER

In the present chapter attention will be given to nonlinear instabilities in a thin annular combustion chamber with uniform injection of liquid propellant (Fig. 3). The unsteady combustion response is characterized by a simple time-delay mechanism which is the same as in a thin rectangular chamber investigated in Chapter 3. For this case the potential function ϕ depends only on θ and t. Therefore, (2.36) can be written as:

$$\phi_{,tt} - \phi_{,\theta\theta} + \varepsilon(\bar{\sigma}((1 - n)\phi_{,t} + n(\phi_T)_{,t}) + 2\phi_{,\theta}\phi_{,\theta t} - \kappa\phi_{,\theta\theta tt}) + O(\varepsilon^2) = 0 \tag{4.1}$$

This potential function predicts the behavior of the amplitudes of the various acoustic modes of the chamber. The velocity potential will be expanded in terms of products of the acoustic normal modes and time-dependent modal amplitudes as follows:

$$\phi(\theta,t) = F_1(t)\cos\theta + F_2(t)\cos 2\theta + \text{----} \tag{4.2}$$

This represents a solution involving standing waves. Traveling waves can also be treated with no essential difficulty, but this matter is not pursued in the present work.

Substituting (4.2) into (4.1), expanding all nonlinear terms in a Fourier cosine-series, and equating the coefficients of cos θ and cos 2θ individually to zero yields,

$$\ddot{F}_1 + F_1 + \varepsilon(\bar{\sigma}((1 - n)\dot{F}_1 + n\dot{F}_{1T}) + 2(F_1\dot{F}_2 + F_2\dot{F}_1) + \kappa\dddot{F}) + 0(\varepsilon^2) = 0 \tag{4.3}$$

$$\ddot{F}_2 + 4F_2 + \varepsilon(\bar{\sigma}((1 - n)\dot{F}_2 + n\dot{F}_{2T}) - F_1\dot{F}_1 + 4\kappa\ddot{F}_2) + 0(\varepsilon^2) = 0 \tag{4.4}$$

These equations are mathematically analogous to the equations obtained by Powell [10] in his investigation of transverse instability in a cylindrical chamber. He obtained numerical solutions to his equations. In what follows the methods of multiple sales will be used to deduce approximate analytical solutions capable of explaining the results computed by Powell [10].

To begin the perturbation procedure let

$$\xi = t \tag{4.5}$$

$$\eta = \varepsilon t \tag{4.6}$$

By using (4.5) and (4.6) equations (4.3) and (4.5) can be readily written as:

$$F_{1,\xi\xi} + F_1 + \varepsilon(2F_{1,\xi\eta} + \kappa F_{1,\xi\xi} + \bar{\sigma}((1 - n)F_{1,\xi} + n(F_{1T})_{,\xi}) + 2(F_1F_{2,\xi} + F_2F_{1,\xi})) + 0(\varepsilon^2) = 0 \tag{4.7}$$

$$F_{2,\xi\xi} + 4F_2 + \varepsilon(2F_{2,\xi\eta} + 4\kappa F_{2,\xi\xi} + \bar{\sigma}((1 - n)F_{2,\xi} + n(F_{2T}),_{\xi})$$

$$- F_1F_1,_{\xi}) + 0(\varepsilon^2) = 0 \tag{4.8}$$

It will now be assumed that the first and second modal amplitudes can be expended in the form

$$F_i = F_{i0} + \varepsilon F_{i1} + \text{----} \tag{4.9}$$

where i can be either 1 or 2.

Substituting (4.9) into (4.7) and (4.8) yields

$$F_{10,\xi\xi} + F_{10} + \varepsilon(2F_{10,\xi\eta} + \kappa F_{10,\xi\xi} + \bar{\sigma}((1 - n)F_{10,\xi}$$

$$+ n(F_{10T}),_{\xi}) + 2(F_{10}F_{20,\xi} + F_{20}F_{10,\xi}) + F_{11,\xi\xi} + F_{11})$$

$$+ 0(\varepsilon^2) = 0 \tag{4.10}$$

$$F_{20,\xi\xi} + 4F_{20} + \varepsilon(2F_{20,\xi\eta} + 4\kappa F_{20,\xi\xi} + \bar{\sigma}((1 - n)F_{20,\xi}$$

$$+ n(F_{20T}),_{\xi}) - F_{10}F_{10,\xi} + F_{21,\xi\xi} + 4F_{21}) + 0(\varepsilon^2) = 0 \tag{4.11}$$

Since F_{10}, F_{11}, F_{20}, and F_{21} do not depend on ε each coefficient of a power of ε must be individually set equal to zero. This yields

$$F_{10,\xi\xi} + F_{10} = 0 \tag{4.12}$$

$$F_{20,\xi\xi} + 4F_{20} = 0 \tag{4.13}$$

$$2F_{10,\xi\eta} + \kappa F_{10,\xi\xi} + \bar{\sigma}((1 - n)F_{10,\xi} + n(F_{10T}),_{\xi})$$

$$+ 2(F_{10}F_{20,\xi} + F_{20}F_{10,\xi}) + F_{11,\xi\xi} + F_{11} = 0 \qquad (4.14)$$

$$2F_{20,\xi\eta} + 4\kappa F_{20,\xi\xi} + \bar{\sigma}((1 - n)F_{20,\xi} + n(F_{20T}),_{\xi})$$

$$- F_{10}F_{10,\xi} + F_{21,\xi\xi} + 4F_{21} = 0 \qquad (4.15)$$

The general solutions of equations (4.12-13) may be written as:

$$F_{i0}(\xi,\eta) = A_{i0}(\eta)\cos i\xi + B_{i0}\sin i\xi \qquad (4.16)$$

where i remains either 1 or 2.

The coefficients A_{i0} and B_{i0} can be determined by substituting (4.16) into (4.14) and (4.15), and equating the coefficients of $\cos\xi$ and $\sin\xi$ in (4.14) and $\cos 2\xi$ and $\sin 2\xi$ in (4.15) individually to zero to eliminate singular terms. This produces

$$\dot{A}_{10} + \tfrac{1}{2}\epsilon(\bar{\sigma}((1 - n)A_{10} + n(A_{10}\cos T - B_{10}\sin T)$$

$$+ A_{10}A_{20} + B_{10}B_{20} + \kappa B_{10}) = 0 \qquad (4.17)$$

$$\dot{B}_{10} + \tfrac{1}{2}\epsilon(\bar{\sigma}((1 - n)B_{10} + n(A_{10}\sin T + B_{10}\cos T))$$

$$+ A_{10}B_{20} - A_{20}B_{10} - \kappa A_{10}) = 0 \qquad (4.18)$$

$$\dot{A}_{20} + \tfrac{1}{2}\epsilon\bar{\sigma}((1 - n)A_{20} + n(A_{20}\cos 2T - B_{20}\sin 2T))$$

$$+ \tfrac{1}{4}(B_{10}^2 - A_{10}^2) + 8\kappa B_{20}) = 0 \qquad (4.19)$$

$$\dot{B}_{20} + \tfrac{1}{2}\epsilon\bar{\sigma}((1 - n)B_{20} + n(A_{20}\sin 2T + B_{20}\cos 2T))$$

$$- \tfrac{1}{2}A_{10}B_{10} - 8\kappa A_{20}) = 0 \qquad (4.20)$$

In obtaining (4.17-20) the identities

$$\cos\xi\sin 2\xi = \tfrac{1}{2}(\sin\xi + \sin 3\xi)$$

$$\cos\xi\cos 2\xi = \tfrac{1}{2}(\cos\xi + \cos 3\xi)$$

$$\sin\xi\sin 2\xi = \tfrac{1}{2}(\cos\xi - \cos 3\xi)$$

were used.

It is convenient to rewrite (4.17-20) in terms of amplitudes C_i and phase angles α_i defined as:

$$A_i = C_i\cos\alpha_i \qquad (4.21)$$

$$B_i = C_i\sin\alpha_i \qquad (4.22)$$

For additional convenience the final equations will be written in terms of C_1, C_2, α_1, and

$$\alpha_{12} = \alpha_2 - 2\alpha_1 \qquad (4.23)$$

Substituting (4.21-23) into (4.17-20) and rearranging yields

$$\dot{C}_1 + \frac{1}{2}\epsilon(\bar{\sigma}C_1(1 - n(1 - \cos T)) + C_1C_2\cos\alpha_{12}) = 0 \qquad (4.24)$$

$$\dot{\alpha}_1 + \frac{1}{2}\epsilon(C_2\sin\alpha_{12} + \bar{\sigma}n\sin T - \kappa) = 0 \qquad (4.25)$$

$$\dot{C}_2 + \frac{1}{2}\epsilon(\bar{\sigma}C_2(1 - n(1 - \cos 2T)) - \frac{1}{4}C_1^2\cos\alpha_{12}) = 0 \qquad (4.26)$$

$$\dot{\alpha}_{12} + \frac{1}{2}\epsilon((\frac{C_1^2}{4C_2} - 2C_2)\sin\alpha_{12} + \bar{\sigma}n(\sin 2T - 2\sin T) - 6\kappa) = 0 \qquad (4.27)$$

The linear stability analysis can be recovered from (4.24-27) by neglecting all nonlinear terms. Inspection of the resulting equation shows that the first mode is stable for

$$n \leq \frac{1}{1 - \cos T} \qquad (4.28)$$

while the second mode is stable for

$$n \leq \frac{1}{1 - \cos 2T} \qquad (4.29)$$

It is desired to investigate situations for which the first mode is linearly unstable while the second mode is linearly stable. That is, situations for which

$$\frac{1}{1 - \cos T} \leq n \leq \frac{1}{1 - \cos 2T} \qquad (4.30)$$

For (4.30) to hold the inequality $\frac{2\pi}{3} \leq T \leq \frac{5\pi}{3}$ must hold. In such cases a limit cycle is possible. Its amplitude can be obtained from (4.24-27) by looking for solutions such that C_1 and C_2 are constants. It can be seen that such solutions exist only if α_{12} is constant (note that α_1, and thus α_2 need not be constant).

Solving the algebraic equations produced by assuming that C_1, C_2, and α_{12} are constants yields

$$C_1 = \frac{2\bar{\sigma}}{\cos\alpha_{12}} \sqrt{(1 - n(1 - \cos 2T))(n(1 - \cos T) - 1)} \qquad (4.31)$$

$$C_2 = \frac{\bar{\sigma}(n(1 - \cos T) - 1)}{\cos\alpha_{12}} \qquad (4.32)$$

$$\tan\alpha_{12} = \frac{6\kappa/\bar{\sigma} + n(2\sin T - \sin 2T)}{3 + n(2\cos T + \cos 2T - 3)} \qquad (4.33)$$

To determine whether or not the solutions of (4.24-27) actually approach the limit cycles discussed above, these equations were solved numerically by the Runge-Kutta method (no closed form solutions being apparent). Because of the C_2 appearing in the denomination of (4.27) it is necessary to use a power-series solution for small times whenever the initial condition $C_2(0) = 0$ is used. The appropriate series expansions can be written as:

$$C_1 = 1 + C_{11}t + O(t^2) \qquad (4.34)$$

$$C_2 = C_{21}t + O(t^2) \qquad (4.35)$$

$$\alpha_1 = \alpha_{11}t + 0(t^2) \tag{4.36}$$

$$\alpha_{12} = \alpha_{121}t + 0(t^2) \tag{4.37}$$

Substituting (4.35-38) into (4.24-27) yields

$$C_1 = 1 - \tfrac{1}{2}\bar{\sigma}\epsilon(1 - n(1 - \cos T))t \tag{4.38}$$

$$C_2 = \tfrac{1}{8}\epsilon t \tag{4.39}$$

$$\alpha_1 = \tfrac{1}{2}\epsilon(\kappa - \bar{\sigma}n\sin T)t \tag{4.40}$$

$$\alpha_{12} = \tfrac{1}{2}\epsilon(3\kappa + \tfrac{1}{2}\bar{\sigma}n(2\sin T - \sin 2T)t \tag{4.41}$$

In order to investigate some aspects of the nonlinear stability problem a considerable amount of numerical calculations were performed. Only the most important conclusions and some typical results will be reported in the remainder of this chapter. These results are presented with the following objectives in mind:

(a) The prediction of stable limit cycles for transverse mode instability.

(b) The determination of the dependence of the amplitudes of the limit cycles upon the combustion parameter n and time-delay T which are given by the steady state solution.

The region of the n - T plane in which limit cycles are expected is shown in Fig. 10. Defining

$$n_1 = \frac{1}{1 - \cos T} \tag{4.42}$$

$$n_2 = \frac{1}{1 - \cos 2T} \tag{4.43}$$

It can be seen that for (4.30) to be satisfied

$$n_1 \leq n \leq n_2 \tag{4.44}$$

Thus the region A B C (where B corresponds to $n = \infty$) is the region of interest. Points A and C can be found from $n_1 = n_2$ or

$$\cos 2T - \cos T = 0 \tag{4.45}$$

In the region $0 \leq T \leq 2\pi$ (4.45) has the roots $T = \frac{2\pi}{3}$ and $\frac{5\pi}{3}$.

To determine whether or not solutions to (4.24-27) actually approached the limit cycles predicted by (4.31-33) a variety of numerical solutions to (4.24-27) were obtained by using a fourth-order Runge-Kutta method. Some typical results are shown in Figures 11-15.

Figures 11 and 12 present results for $T = 150°$, $n = 0.65$, and $\kappa = 0$. Substituting these values into (4.31-33) yields

$$\alpha_{12} = 1.368 \text{ Rad.} \tag{4.46}$$

$$C_1 = 3.768\bar{\sigma} \tag{4.47}$$

$$C_2 = 1.058\bar{\sigma} \tag{4.48}$$

for the limit-cycle values.

It can be seen that the numerical results do approach the limit-cycle values and that these are in agreement with (4.46-48). It was established that other sets of initial conditions lead to the same limit cycles. The results of the computations used to establish this fact are not shown.

Figure 13 shows some typical results for $T = \pi$ and $\kappa = 0$. In this case it is possible to simplify (4.24-27) to

$$\dot{C}_1 + \tfrac{1}{2}\epsilon(\bar{\sigma}C_1(1 - 2n) + C_1C_2\cos\alpha_{12}) = 0 \tag{4.49}$$

$$\dot{\alpha}_1 + \tfrac{1}{2}\epsilon C_1C_2\sin\alpha_{12} = 0 \tag{4.50}$$

$$\dot{C}_2 + \tfrac{1}{2}\epsilon(\bar{\sigma}C_2 - \tfrac{1}{4}C_1^2\cos\alpha_{12}) = 0 \tag{4.51}$$

$$\dot{\alpha}_{12} + \tfrac{1}{2}\epsilon(\left(\frac{C_1^2}{4C_2} - 2C_2\right)\sin\alpha_{12} = 0 \tag{4.52}$$

For the initial conditions $\alpha_1(0) = \alpha_{12}(0) = 0$, (4.50) and (4.52) are satisfied by

$$\alpha_1 = \alpha_{12} = 0 \tag{4.53}$$

Substituting (4.53) into (4.49) and (4.51) yields

$$\dot{C}_1 + \tfrac{1}{2}\epsilon(\bar{\sigma}(1 - 2n)C_1 + C_1C_2) = 0 \tag{4.54}$$

$$\dot{C}_2 + \tfrac{1}{2}\epsilon(\bar{\sigma}C_2 - \tfrac{1}{4}C_1^2) = 0 \tag{4.55}$$

Thus α_1 and α_{12} can be determined in close-form and C_1 and C_2 must be determined numerically from (4.54) and (4.55). For these conditions (4.31-33) simplify to

$$C_1 = 2\bar{\sigma}\sqrt{2n - 1} \tag{4.56}$$

$$C_2 = \bar{\sigma}(2n - 1) \tag{4.57}$$

$$\alpha_{12} = 0 \tag{4.58}$$

It can be seen that (4.56-57) are consistent with (4.54-55).

The numerical results shown in Figure 13 are for n = 1. It can be seen that the correct limit-cycle values are approached for large t. No difficulty was encountered in getting the numerical solutions to approach the limit-cycle values given by (4.54-55) for any value of n tried. This is in contrast to the situations for $T \neq \pi$. This will be discussed below.

For values of T other than 180° there appeared to be an upper limit on the value of n for which the numerical solutions would approach the limit-cycle values given by (4.31-33). (The upper limit appeared to be approximately $n_u = 0.75$, but more work would be required to make this value more definitive.) For $n > n_u$ numerical calculations indicate that $C_1 \to \infty$ and $C_2 \to \infty$ as $t \to \infty$. Inspection of the numerical results showed that C_1 and C_2 would come close to the limit-cycle values for intermediate values of time, but then diverge from these values because α_{12} would pass the limit-cycle values and continue growing. Thus it is suspected that $n_u = \infty$ for T = 180° and $\kappa = 0$ because $\alpha_{12}(t) = 0$ for

these conditions. Thus α_{12} is already at its limit-cycle value and remains there for all t. It is suspected that the limit cycle is unstable for $n>n_u$. A linear stability analysis could be carried out in an attempt to verify this conjecture, but this was not done in the present work.

To make sure that the lack of approach to the limit cycle discussed above was not due to errors in the numerical procedure, the following method was used. A value of α_{12} was selected, and (for given values of T, $\bar{\sigma}$, and $n>n_u$) the corresponding value of κ was found from (4.33). Then the appropriate values of C_1 and C_2 were found from (4.31-32). Then a numerical solution was found by using these values of C_1, C_2, and α_{12} as the initial conditions. It was found that in these cases the variables remained constant at their initial values. Results of two typical calculations of this type are shown in Figures 14 and 15. It was also observed that the slighest deviation of the initial values from those computed by the procedure described above lead to divergence of the variables from their limit-cycle values. This behavior provides further support for the conjecture that the limit cycles are unstable for $n>n_u$.

It should be noted that for $\kappa = 0(1)$ the frequency of the second acoustic mode is very nearly twice the frequency of the first acoustic mode. The perturbation method makes it clear that the existence of a limit cycle depends critically on this fact. This is not evident from the numerical solution found by Powell [10].

Chapter 5

CONCLUSION

In this report the two-variable perturbation method was used to solve the modal-amplitude equations arising from the application of the Galerkin method to a nonlinear wave equation describing pressure-sensitive combustion-instability problems in liquid-fuel rocket motors. Two idealized problems were discussed. The first was that of transverse symmetric motion in a narrow rectangular combustion chamber. This problem exhibits self-coupled instability. The second was that of transverse motion in a narrow annular combustion chamber. This problem exhibits mode-coupled instability. In this way an application of the method to each type of pressure-sensitive instability problem was presented.

For the case of the rectangular chamber both the linear and nonlinear stability boundaries and limit-cycle amplitudes were obtained in closed form. It was also possible to determine the evolution of the initial disturbance in closed form after making a slight approximation. When this approximation was removed a numerical solution was required to determine this evolution.

For the case of the annular combustion chamber the linear stability boundaries and the limit-cycle amplitudes were found in closed form. The evolution of the initial disturbance was determined numerically.

In both cases the results exhibited the same behavior as that observed by Powell [10] who used direct numerical solution of the modal-amplitude equations to analyze similar problems. In fact it was found that the closed-form solutions obtained herein could be used to explain several of the parametric trends observed in [10]. Since the functions determined numerically in the present work are much simpler than those computed in [10] it is thought that present procedure offers opportunities for significant savings of computer time.

On the basis of the numerical results the following nonlinear mechanisms were found to be important in determining the nonlinear stability characteristics of the system: (a) the transfer of energy between modes and (b) the self coupling of a mode with itself.

LIST OF REFERENCES

1. Sotter, J. G., and Flandro, G. A., "Resonant Combustion in Rockets," Scientific American, December 1968, pp. 95-103.

2. Crocco, L., and Cheng, S. I., Theory of Combustion Instability in Liquid Propellant Rocket Motors, AGARD Monograph No. 8, Butterworths Scientific Pub. Ltd., London, 1956.

3. Scala, S. M., "Transverse Wave and Entropy Wave Combustion Instability in Liquid Propellant Rockets," Princeton University Aeronautical Engineering Report No. 380, April 1957 (Ph.D. Thesis).

4. Reardon, F. H., "An Investigation of Transverse Mode Combustion Instability in Liquid Propellant Rocket Motors," Princeton University Aeronautical Engineering Report No. 550, June 1961 (Ph.D. Thesis).

5. Culick, F. E. C., "Stability of High Frequency Pressure Oscillations in Gas and Liquid Rocket Combustion Chambers," M.I.T. Aerophysics Laboratory Report No. 480, June 1961.

6. Zinn, B. T., "A Theoretical study of Nonlinear Transverse Combustion Instability in Liquid Propellant Rocket Motors," Princeton University AMS Technical Report No. 732, May 1966 (Ph.D. Thesis).

7. Maslen, S. H., and Moore, F. K., "On Strong Transverse Waves Without Shocks in a Circular Cylinder," Journal of Aeronautical Sciences, Vol 23, No. 6, 1956, pp. 583-593.

8. Priem, R. J., and Guentert, D. C., "Combustion Instability Limits Determined by a Nonlinear Theory and a One-dimensional Model," NASATN D-1409, October 1962.

9. Burstein, S. Z., and Chinitz, W., "Nonlinear Combustion Instability in Liquid Propellant Rocket Motors," Jet Propulsion Laboratory Quarterly Reports prepared under contract 951946.

10. Powell, E. A., "Nonlinear Combustion Instability in Liquid Propellant Rocket Engines," Georgia Institute of Technology, September 1970 (Ph.D. Thesis).

11. Nayfeh, A. H., "Perturbation Methods," Pure and Applied Mathematics, A Wiley-Interscience Series of Texts, Monographs and Tracts, May 1972.

APPENDIX

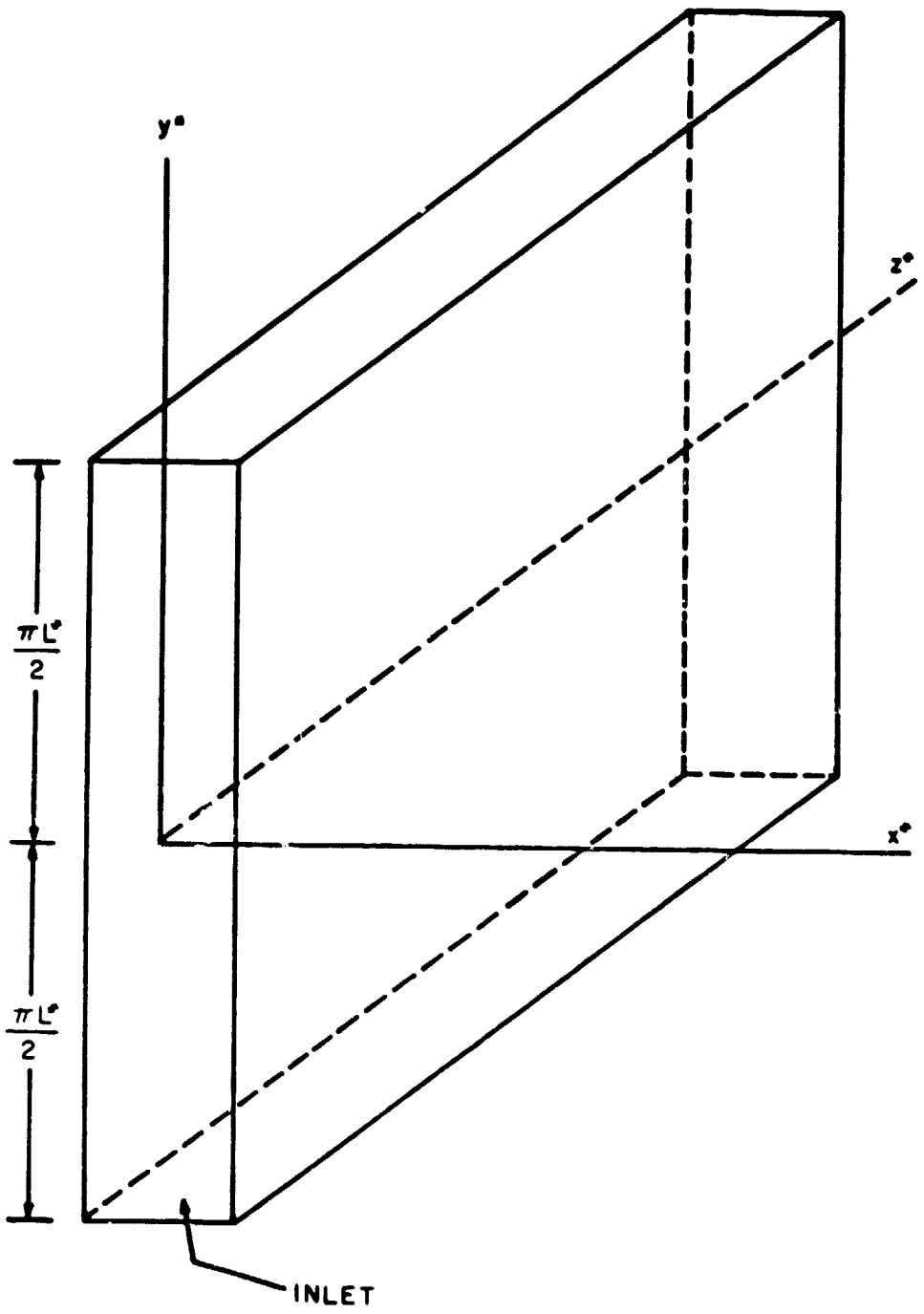

Figure 1. Geometry and Coordinate System for Rectangular Chamber

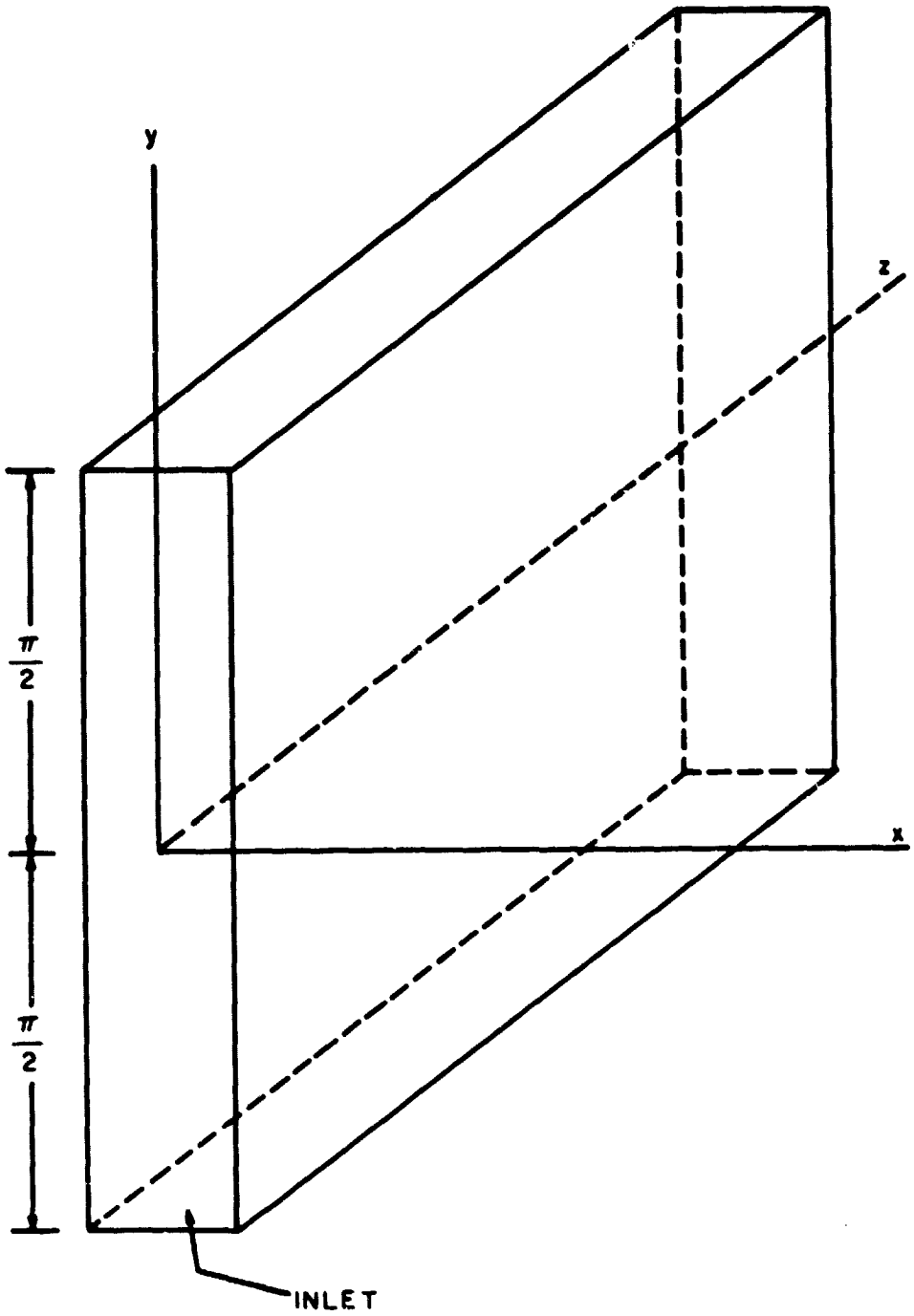

Figure 2. Geometry and Dimensionless Coordinate System for Rectangular Chamber

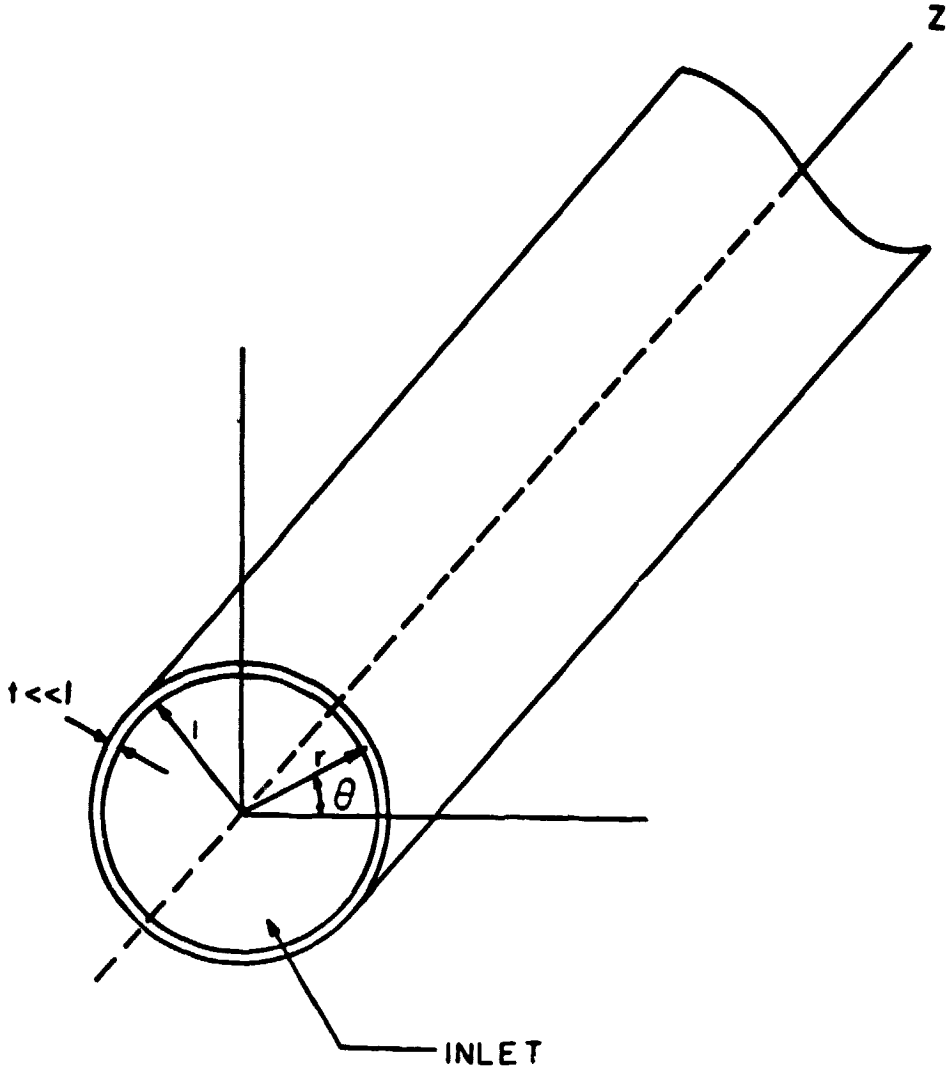

Figure 3. Geometry and Dimensionless Coordinate System for Annular Chamber

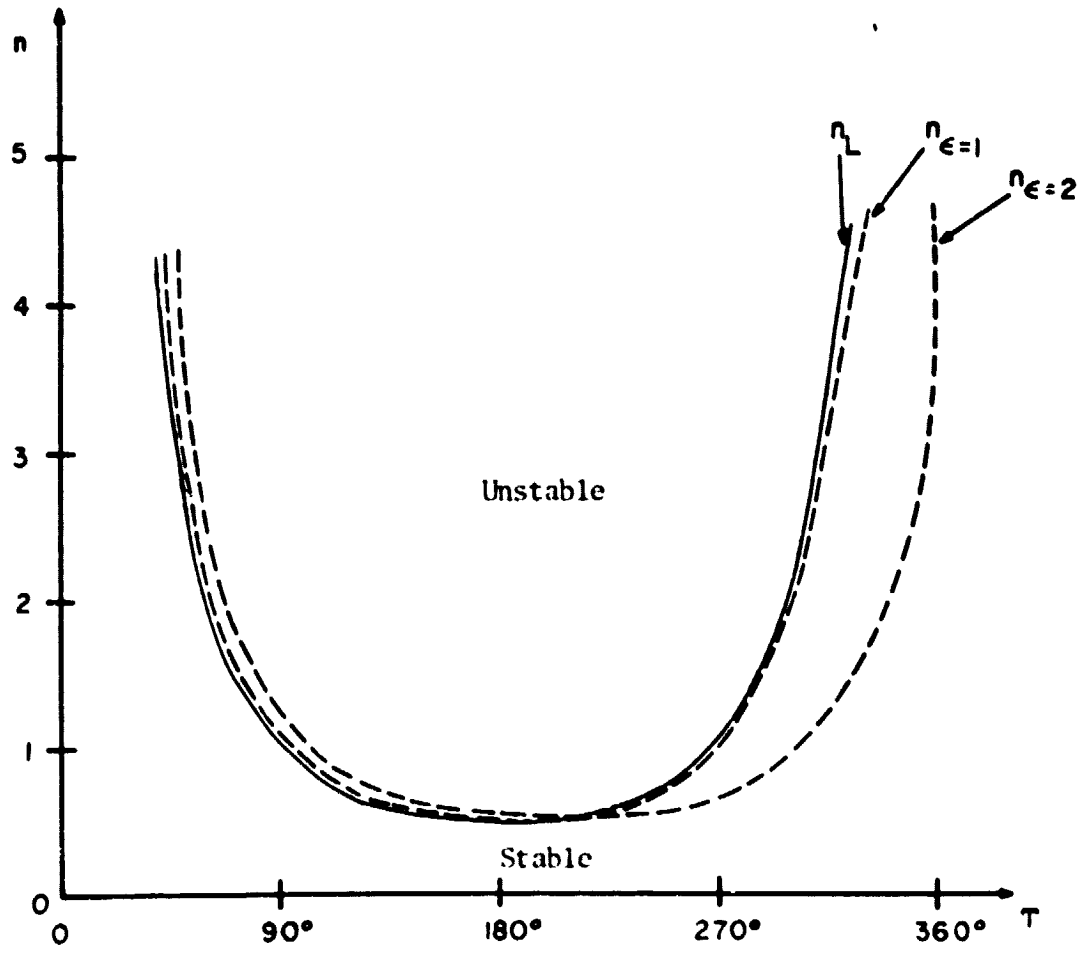

Figure 4. Stability Boundaries for Rectangular Chamber (exact theory)

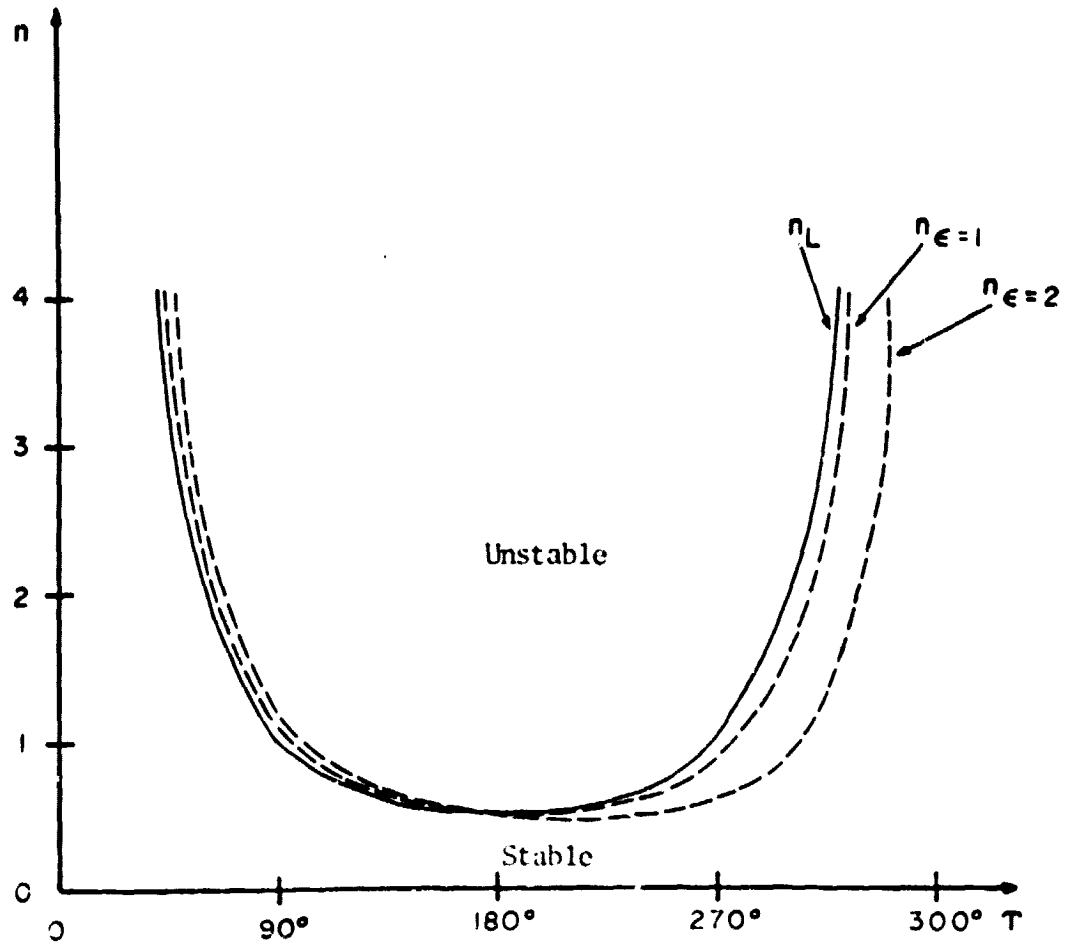

Figure 5. Stability Boundaries for Rectangular Chamber (approximate theory)

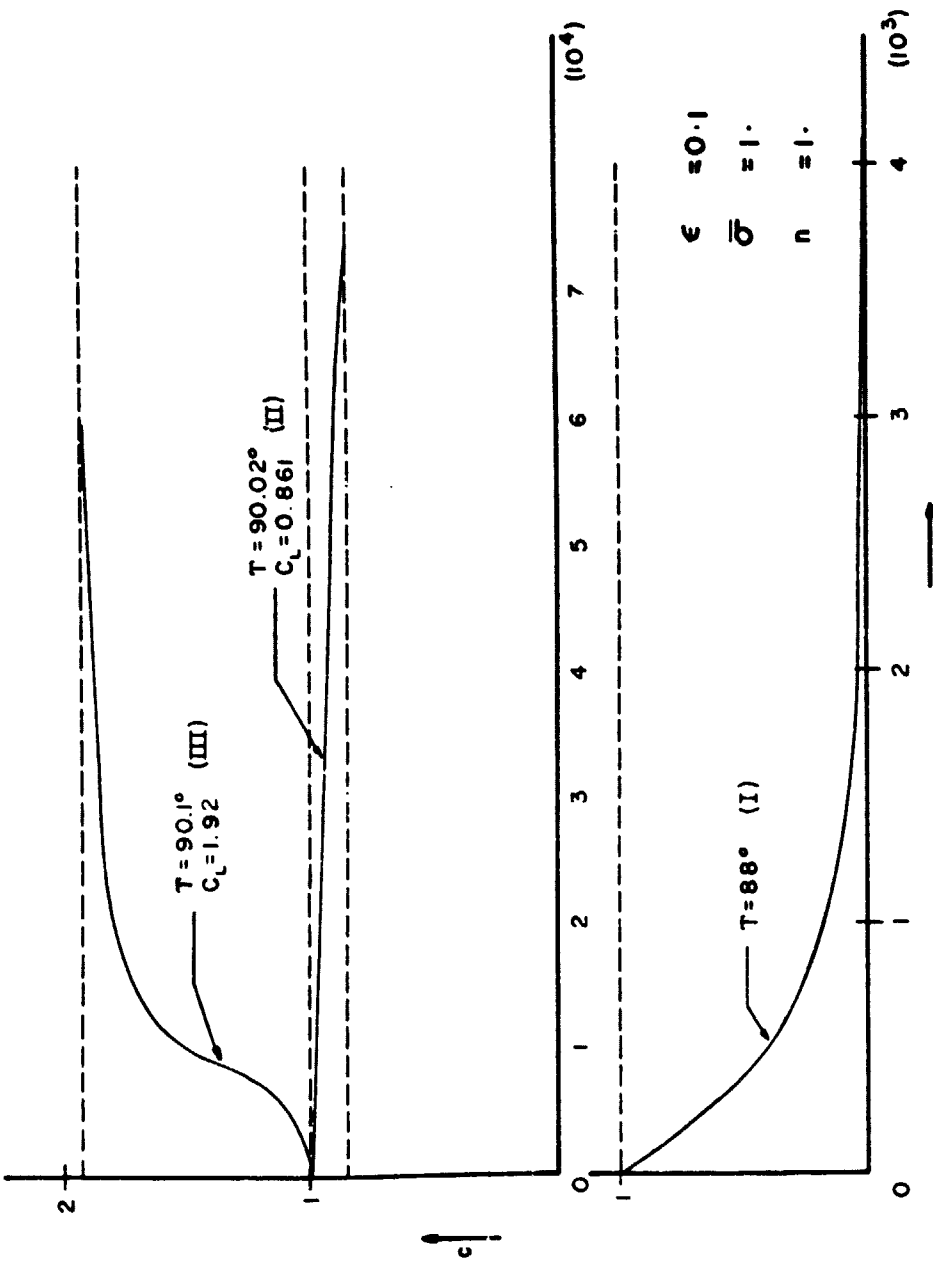

Figure 6. Modal Amplitudes Versus Time for Rectangular Chamber

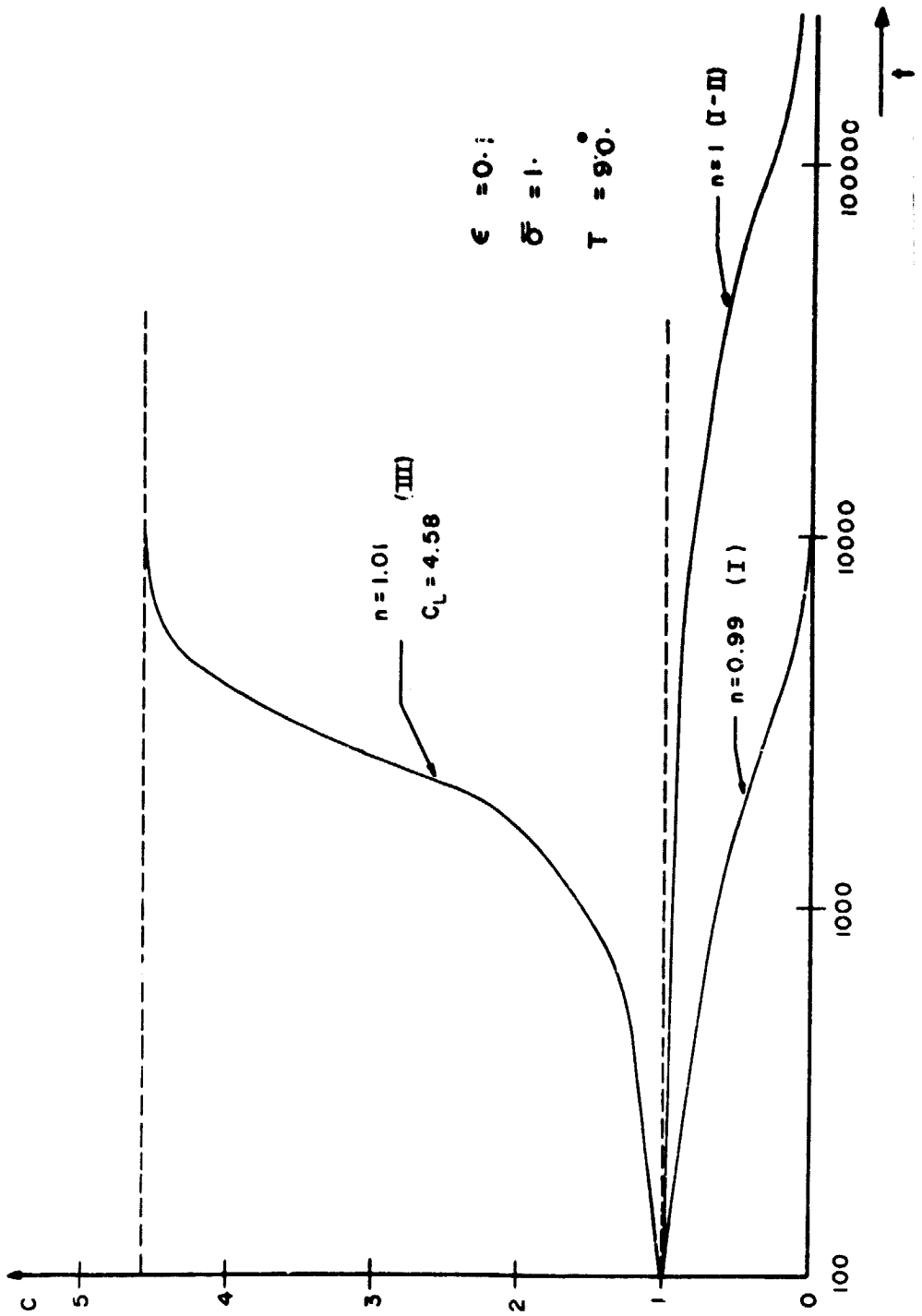

Figure 7. Modal Amplitudes Versus Time for Rectangular Chamber

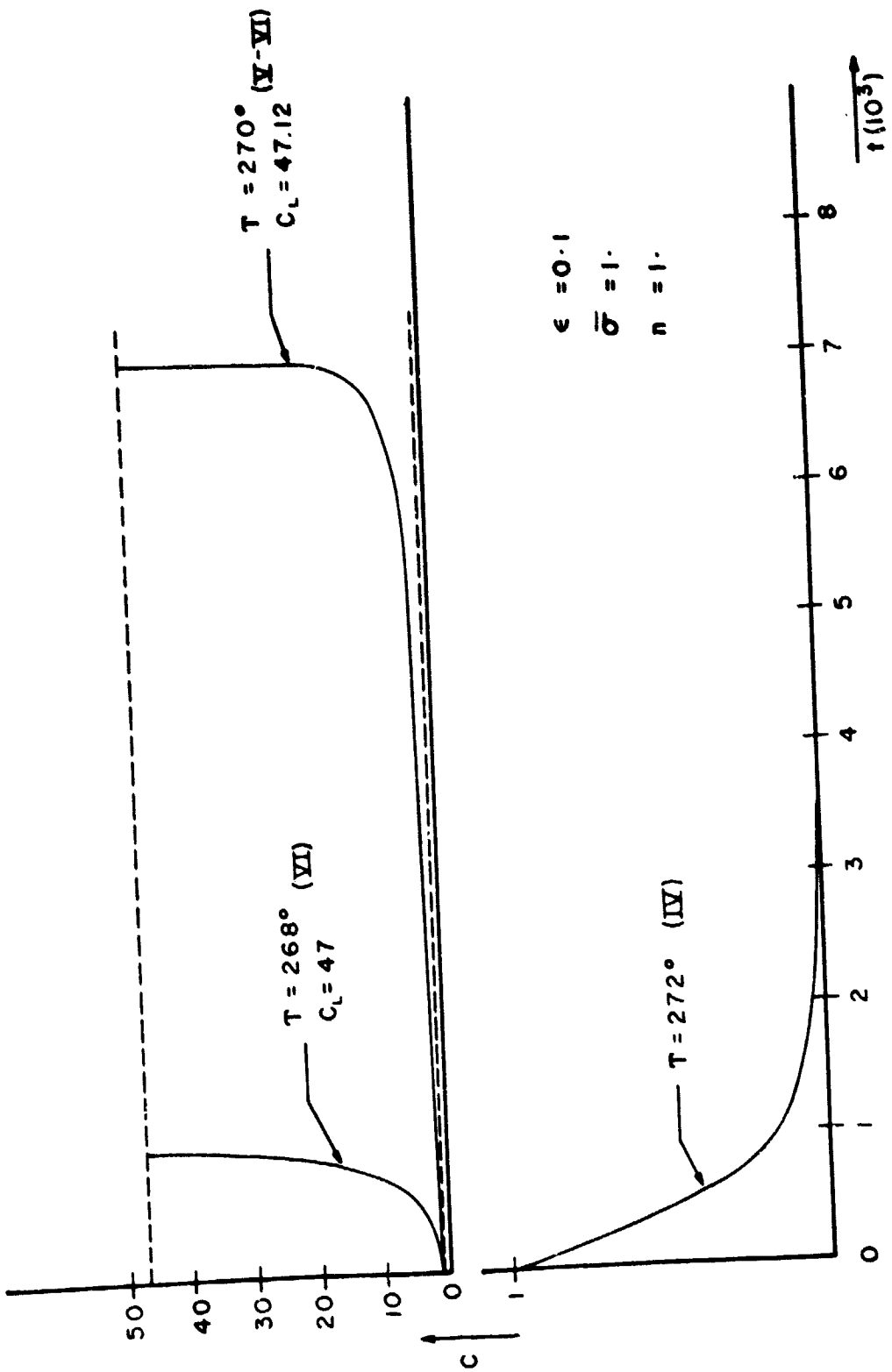

Figure 8. Modal Amplitudes Versus Time for Rectangular Chamber

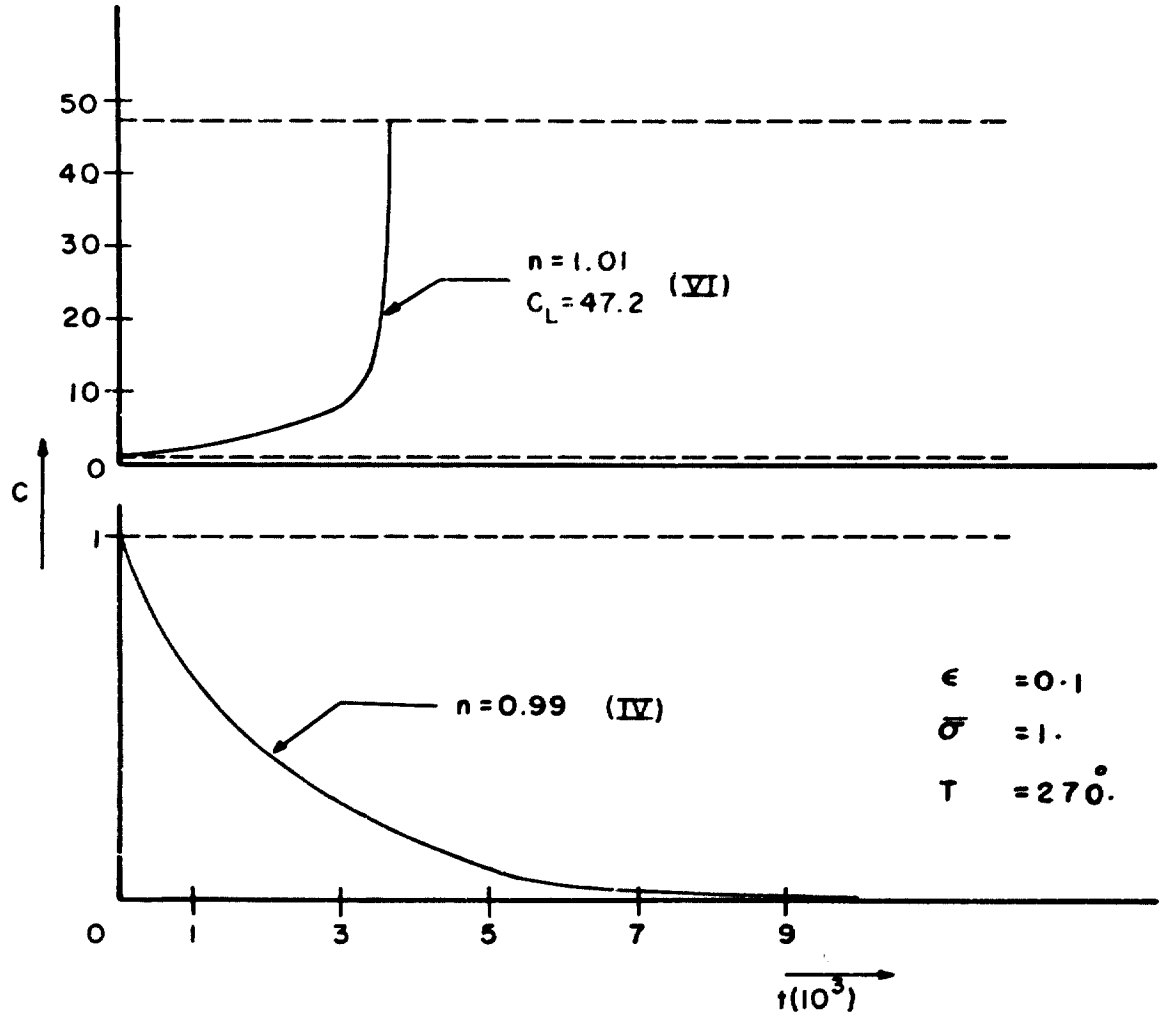

Figure 9. Modal Amplitudes Versus Time for Rectangular Chamber

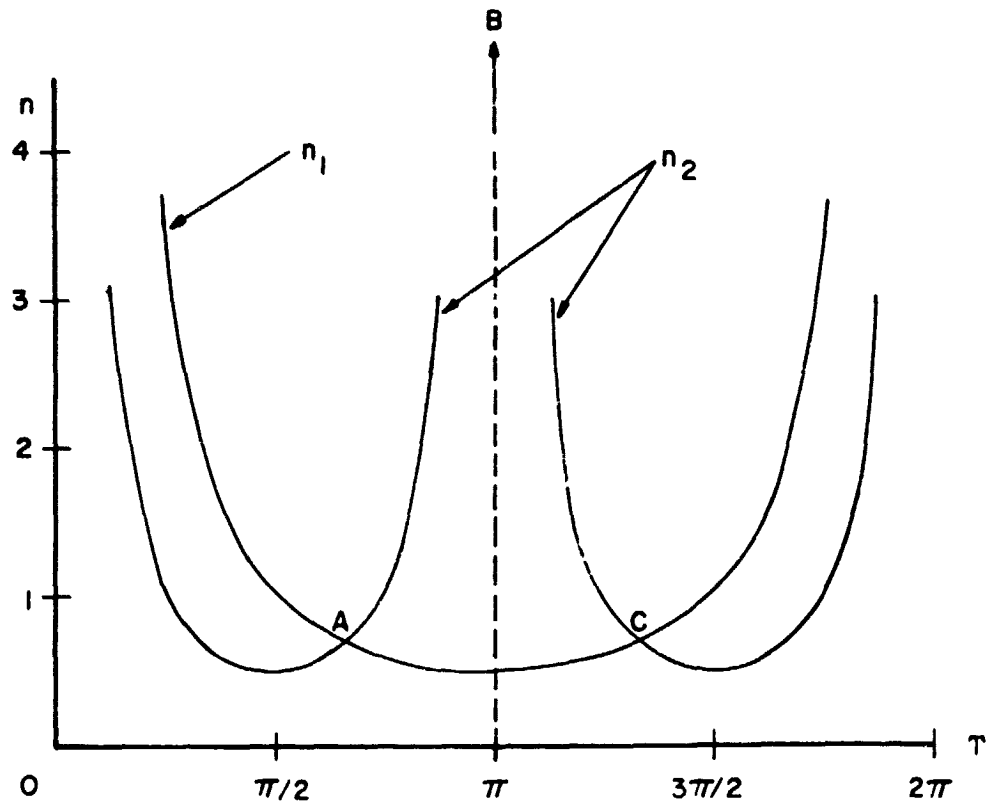

Figure 10. Linear Stability Boundaries for Annular Chamber

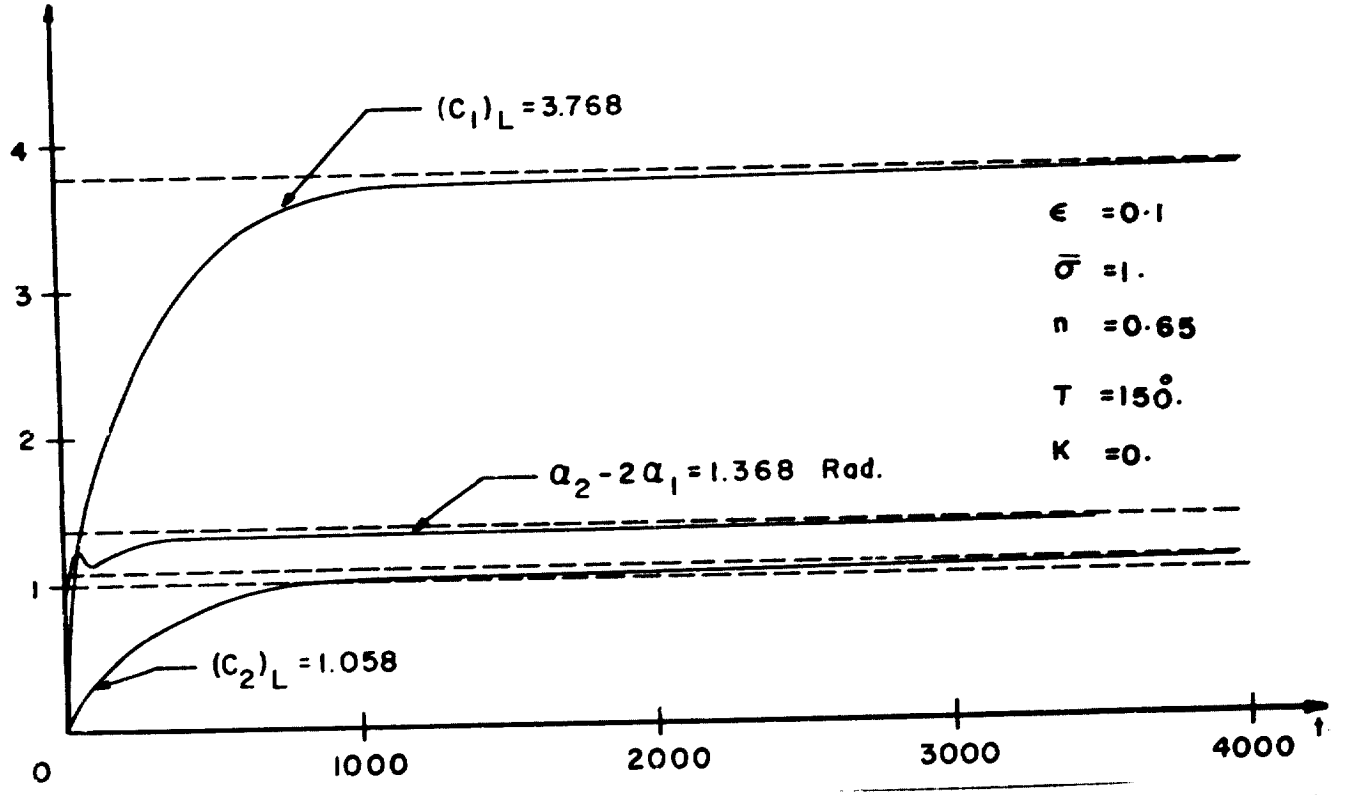

Figure 11. Modal Amplitudes and Phase-Angle Difference Versus Time for Annular Chamber

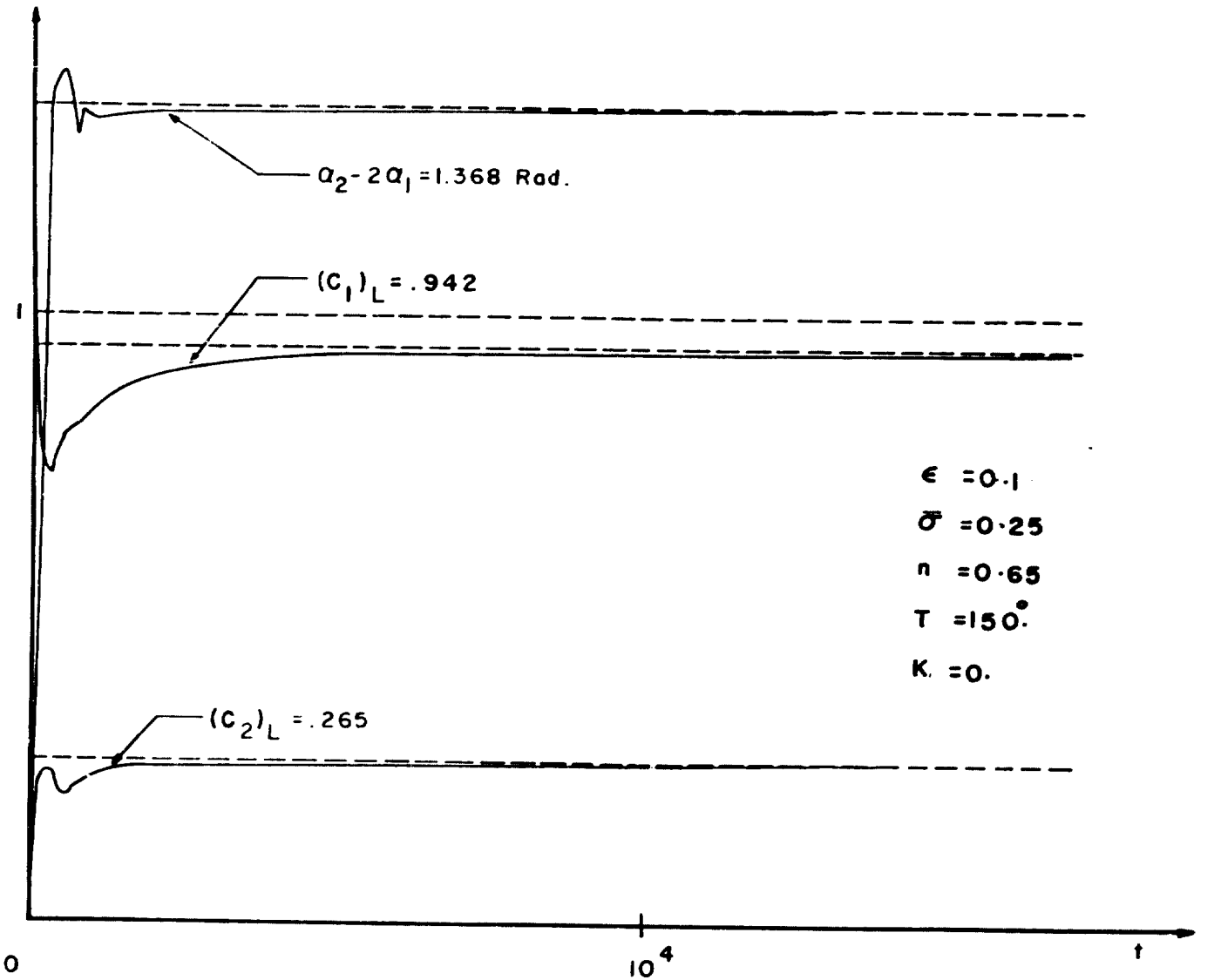

Figure 12. Modal Amplitudes and Phase-Angle Difference Versus Time for Annular Chamber

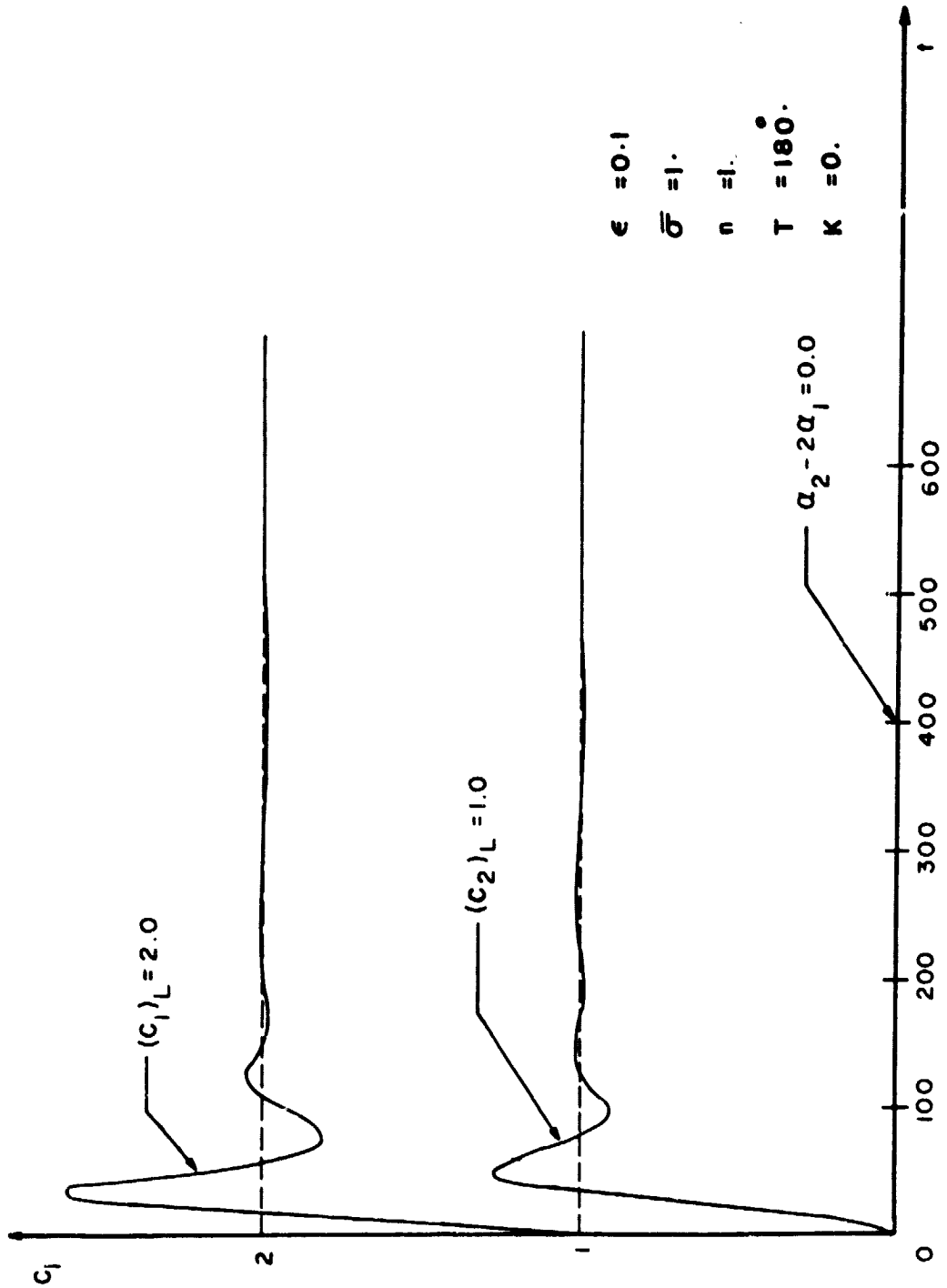

Figure 13. Modal Amplitudes and Phase-Angle Difference Versus Time for Annular Chamber

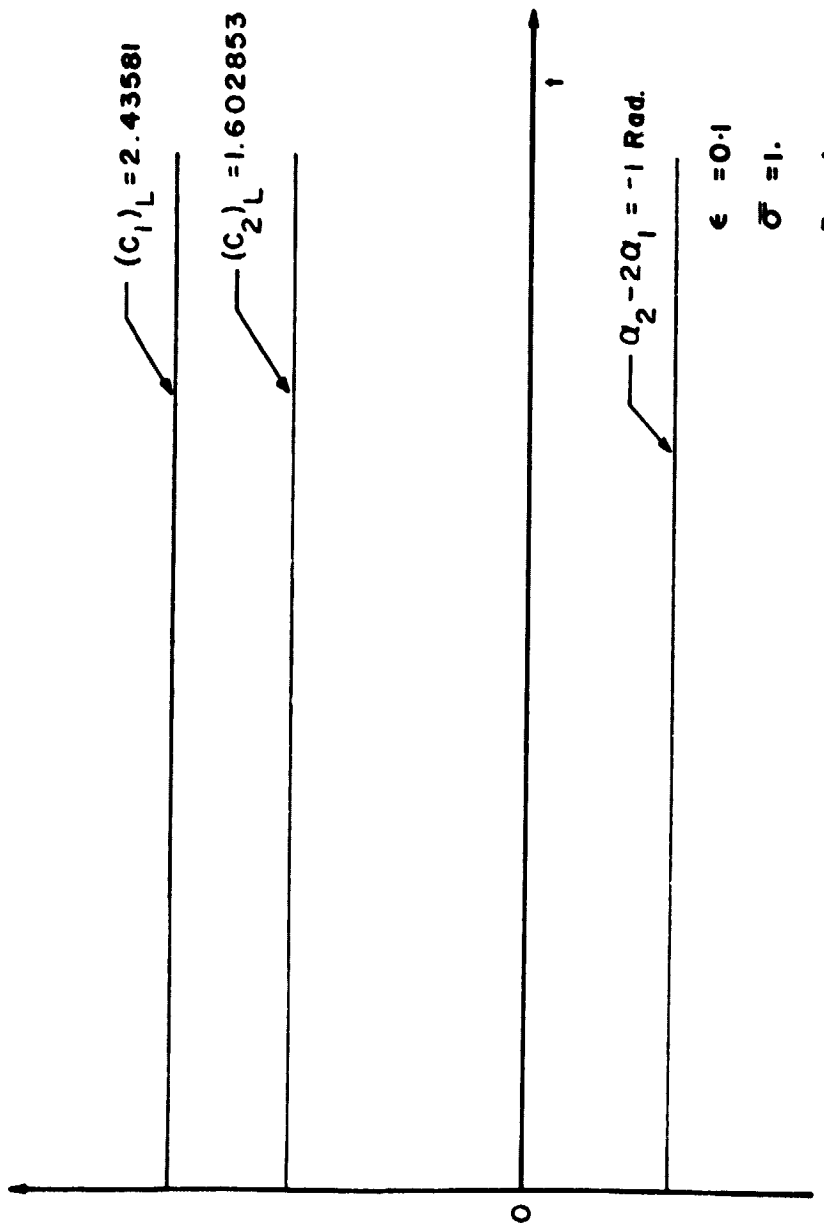

Figure 14. Modal Amplitudes and Phase-Angle Difference Versus Time for Annular Chamber

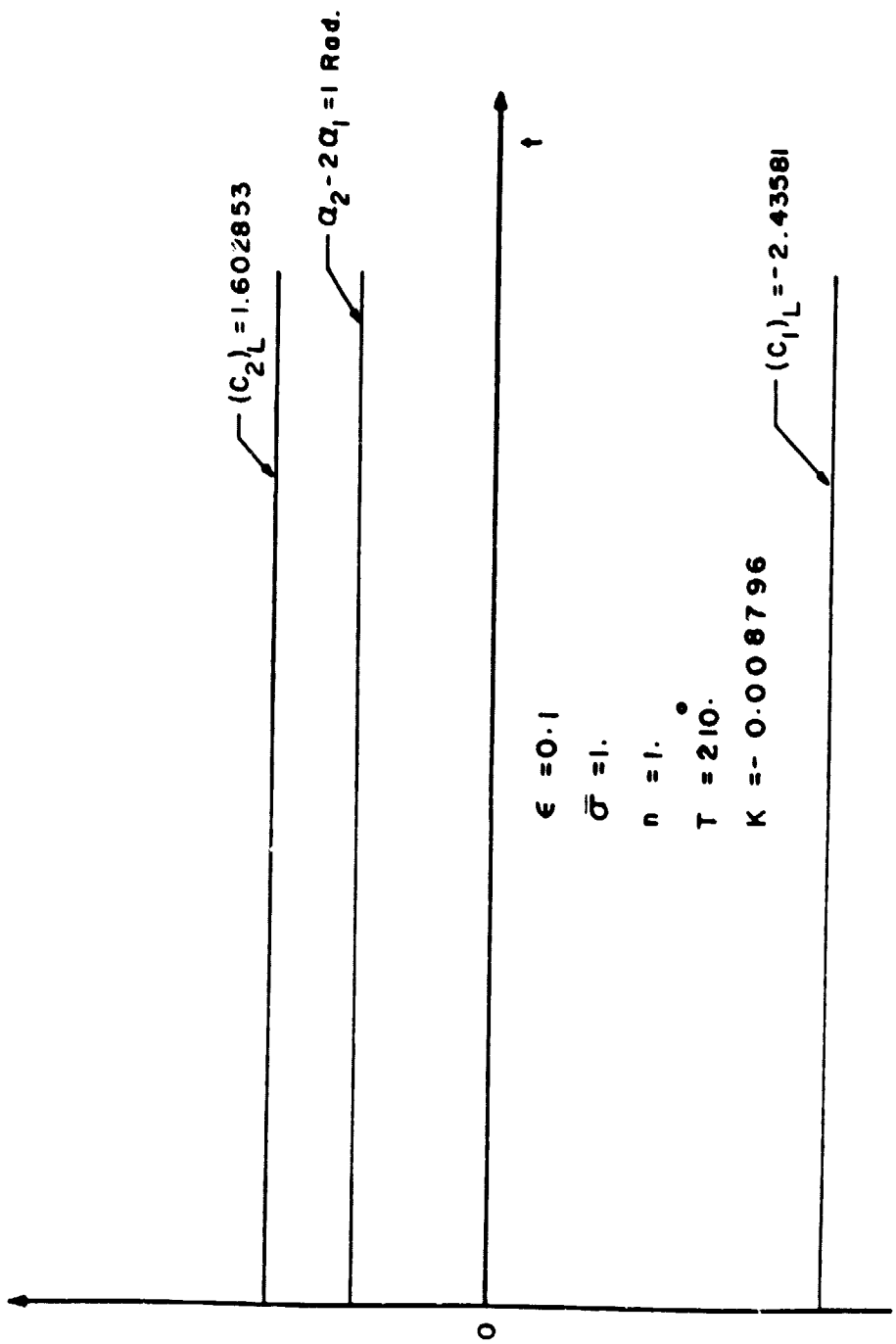

Figure 15. Modal Amplitudes and Phase-Angle Difference Versus Time for Annular Chamber